Acta Geochim (2023) 42:912–933
https://doi.org/10.1007/s11631-023-00624-8

ORIGINAL ARTICLE

Geochronology and geological significance of the strata of the Neoproterozoic Nanhua System, SW North China Craton

Guanxu Chen[1] · Luo Jinhai[2] · Sun Gennian[1] · Meng Zhan[3] · Chang Yinglei[2] · Chen Zhuo[2]

Received: 9 March 2023 / Revised: 5 June 2023 / Accepted: 20 June 2023 / Published online: 4 July 2023

Abstract A set of low-grade clastic metamorphic and carbonate rocks, and greenschists outcropping in the southwestern (SW) margin of the North China Craton (NCC), was originally classified as the Paleoproterozoic Xiong'er Group according to stratigraphic correlation. To verify the age, this paper carried out detrital zircon U–Pb LA-ICP-MS dating of low-grade clastic metamorphic rocks exposed in the Changqing area at the SW margin of the Ordos Block in the SW part of the NCC. Results from detrital zircon dating indicate that the metamorphic and carbonate rocks can be classified into the Neoproterozoic Nanhua System, which is the only Nanhua System stratum in this block so far, and it probably could provide new clues to Rodinia break-up and Snowball Earth of the NCC. The nine peak ages of the low-grade clastic metamorphic rocks reflected its relatively complex provenance, and almost all major geological events experienced by the NCC basement since the Neoarchean, but some age peaks were difficult to correspond to that of the NCC, indicating that the southwestern part of the Ordos Block was also affected by the Qinling and Qiliang orogenic belts during Nanhua System of Neoproterozoic. Combined with provenance analysis, it was revealed that the current southwest boundary of the Ordos Block was the previous southwest boundary of the Ordos Block during the Qingbaikou-Nanhua Period of the Neoproterozoic.

Keywords The Ordos Block · Low-grade metamorphic rocks · Zircon U–Pb age · Paleoproterozoic · Neoproterozoic Nanhua System

✉ Luo Jinhai
luojh@nwu.edu.cn

1 School of Geography and Tourism, Shaanxi Normal University, Xi'an 710119, China

2 State Key Laboratory of Continental Dynamics, Department of Geology, Northwest University, Xi'an 710069, China

3 Yanchang Oil Co., Ltd, Xi'an 71600, China

1 Introduction

The original Paleoproterozoic Xiong'er Group (Fig. 1) in Changqing town in the Southwestern (SW) Ordos Block of the SW North China Craton (NCC) is mainly composed of a set of greenschists (the Changqing greenschists) and low-grade clastic metamorphic rocks and carbonate (the Changqing low-grade clastic metamorphic rocks and carbonate, Pt_3C). The greenschists are in contact with the low-grade clastic metamorphic rocks and carbonate by a normal fault and located on the hanging wall of the fault (Fig. 2), and hence, these metamorphic rocks cannot form a uniform rock-stratigraphic unit. So far, accurate chronological data about these metamorphic rocks are absent, and their depositional environment and structural significance are not clear. According to zircon U–Pb dating results of the greenschists (Chen 2019) and the clastic interbedded rock in the greenschists (Chen et al. 2019), the formation age of the greenschist protolith was restricted to Late Triassic-Early Jurassic. So, the greenschists should be disintegrated from the Xiong'er Group of Paleoproterozoic. In this case, whether the epiclastic metamorphic carbonate rocks still belong to the Xiong'er Group is worthy of further study. You (2016) provided $^{207}Pb/^{206}Pb$ ages of 1091 ± 46 Ma – 2854 ± 170 Ma using U–Pb LA-ICP-MS dating of detrital zircon on a low-grade metamorphic sandstone sample,

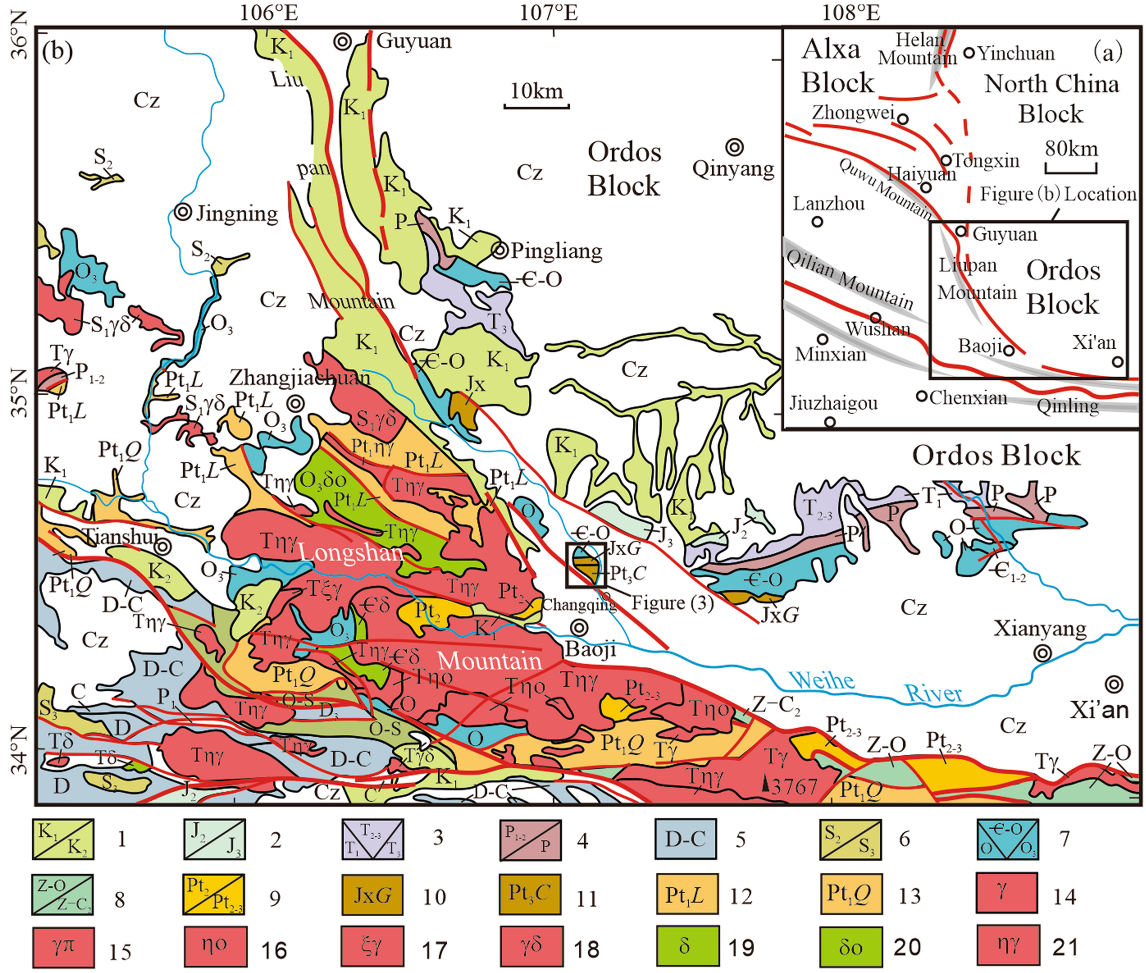

Fig. 1 Simplified geological map of the southwestern margin of the Ordos Block, China and its adjacent area. 1. Lower Cretaceous/Upper Cretaceous; 2. Middle Jurassic/Upper Jurassic; 3. Lower Triassic/Middle Triassic/Lower Triassic; 4. Permian system/Lower Permian/Middle Permian; 5. Devonian System-Carboniferous System; 6. Middle Silurian/Upper Silurian; 7. Ordovician System/Cambrian system-Ordovician System/Upper Ordovician; 8. Sinian System-Ordovician System/Sinian System-Middle Cambrian. 9. Mesoproterozoic/Mesoproterozoic-Upper Proterozoic; 10. Guandaokou Group of Jixian System of Mesoproterozoic; 11. Neoproterozoic Changqing low-graded metamorphic rocks in this paper; 12. Palaeoproterozoic Longshan Group; 13. Palaeoproterozoic Qinlong Group; 14. Granite; 15. Granite porphyry; 16. Quartz monzonite; 17. Syenogranite; 18. Granodiorite; 19. Diorite; 20. Quartz diorite; 21. Monzonitic granite

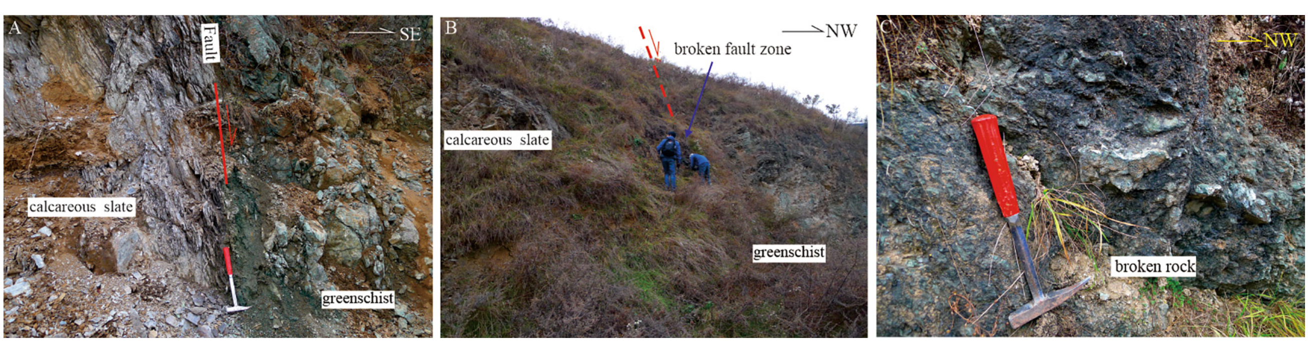

Fig. 2 Representative field photos of the normal fault between the low-graded metamorphic clastic rock-carbonate and greenschist; A. Fault contact between the greenschist and calcareous slate; B. Prospect of the contact zone between the greenschist and calcareous slate; C. Partial enlarged photo of the fault cataclastic rock

indicating the deposition time of the metasandstone protolith should be later than 1091 Ma, and this time is markedly later than the formation time of the typical Xiong'er Group (1.80–1.75 Ga, Zhao 2004; 1.80–1.78 Ga, Zhai et al. 2014) outcropping in the southern part of the NCC. Thus, the preliminary determination is that the low-grade metamorphic sandstone should not be classified as the Xiong'er Group. In this research, based on a detailed geological field survey in the Changqing area, detrital zircon U–Pb LA-ICP-MS dating analyses of multiple samples of low-grade clastic metamorphic rocks were performed to further constrain the formation time of this stratum. Further, we reveal the characteristics of the provenance area of the clastic rocks and discuss the regional structural characteristics of this set of low-grade clastic metamorphic rocks-carbonate when they were deposited.

2 The geological background and petrological characteristics

The Changqing low-grade clastic metamorphic rock-carbonate is not widely exposed in the south of the Fengjiashan reservoir and is mainly exposed on both banks of the Qianhe River. The area around these rocks is mainly covered by the Quaternary system. At two outcrops on both sides of the riverbed, it can be seen that the rocks are in contact with the Upper Triassic-Lower Jurassic greenschists as a normal fault, where the schists are located in the hanging wall, and the metamorphic rock-carbonate in the footwall of the normal fault (Figs. 2a, b, c and 3). Since the top and bottom interfaces of the low-grade clastic metamorphic rock-carbonate are not exposed, the thickness of this set of strata is unknown, and the exposed thickness is about 1000 m.

The low-grade clastic metamorphic rock-carbonate assemblage is mainly composed of limestone, marbled limestone, gray-black sericite slate, calcareous slate, and phyllite, intercalated with multiple layers of conglomerate and glutenite (Fig. 4). The gray-white calcareous slate is about 10–15 cm thick, with plate structures, no recrystallized minerals visible to the naked eye, and very fine sericite locally. The variable residual bedding structure is retained in the rock, and the degree of metamorphism is relatively low.

Gray-black sericite slate and calcareous slate are mainly exposed on the eastern bank of the Qianhe River, occasionally intercalated with thin-layer quartzite, forming an anticline structure, with an anticline junction occurrence of 103°∠15° (Figs. 4c and 5a). The western bank of the Qianhe River mainly exposes gray-black slate, middle-thin marble, and limestone, with multiple layers of gray-black, gray-white conglomerate, sandstone, and blastopsammite, forming a south-dipping monoclinic structure. The conglomerate has a complex gravel composition, mainly sandstone, limestone, metamorphic rock, etc. Gravels are sub-angular, poorly sorted, and the maximum diameter is about 5 cm (Fig. 5b).

The blastopsammite is gray-white as a whole, with a medium-thick layered shape, and the original sedimentary bedding can be seen. The fresh side of the rock is pale gray. According to thin-section observation (Fig. 6), the rock is supported by particles and has a variable sand-like structure with porous cementation. The content of debris is about 90%, sorting is relatively poor, and roundness is low (subangular). Mineral–mineral combinations are arranged in micro-directional arrangements, with the main components as quartz (∼ 45%), rock fragments (∼ 40%), a small fraction of mica, and other minerals (less than 5%). The rest are heterobase and cement (∼ 10%). The composition of the rock fragments is relatively complex with mainly carbonate rock fragments, in addition to some sandstone and limestone detritus. The particle size of the detritus is not more than 3 mm, quartz presents a granular shape, where most of the particles have wavy extinction and the grains are small, with a particle size of 0.025–0.12 mm. Argillaceous and silicalite are the main interstitials with a small amount of iron oxide and calcium. It is named lithic quartz sandstone according to its mineral composition.

From the thin-section study, it can be observed that the sorting and roundness of clastic particles are relatively poor, the content of detritus is very high, and the detritus is mainly carbonate. This reflects that the compositional maturity and structural maturity are relatively low, indicating that it is the product of near-source accumulation and that the provenance may be the coastal area adjacent to the active structural zones.

3 Analysis methods

Two samples of variable residual sandstone and one sample of quartzite (Fig. 5a b for sampling locations) were selected at the Regional Geological Survey Institute of Langfang City, Hebei Province. For the sorted zircon, non-cracked, colorless, and transparent particles under binoculars were selected, then fixed with epoxy resin, and polished until half of the zircon particles were exposed. Cathodoluminescence (CL) photography was then performed to reflect the internal structure of zircon. LA-ICP-MS *in-situ* isotope and trace element analysis and testing were further carried out. Zircon U–Pb dating, CL photography, and trace element analyses were completed in the

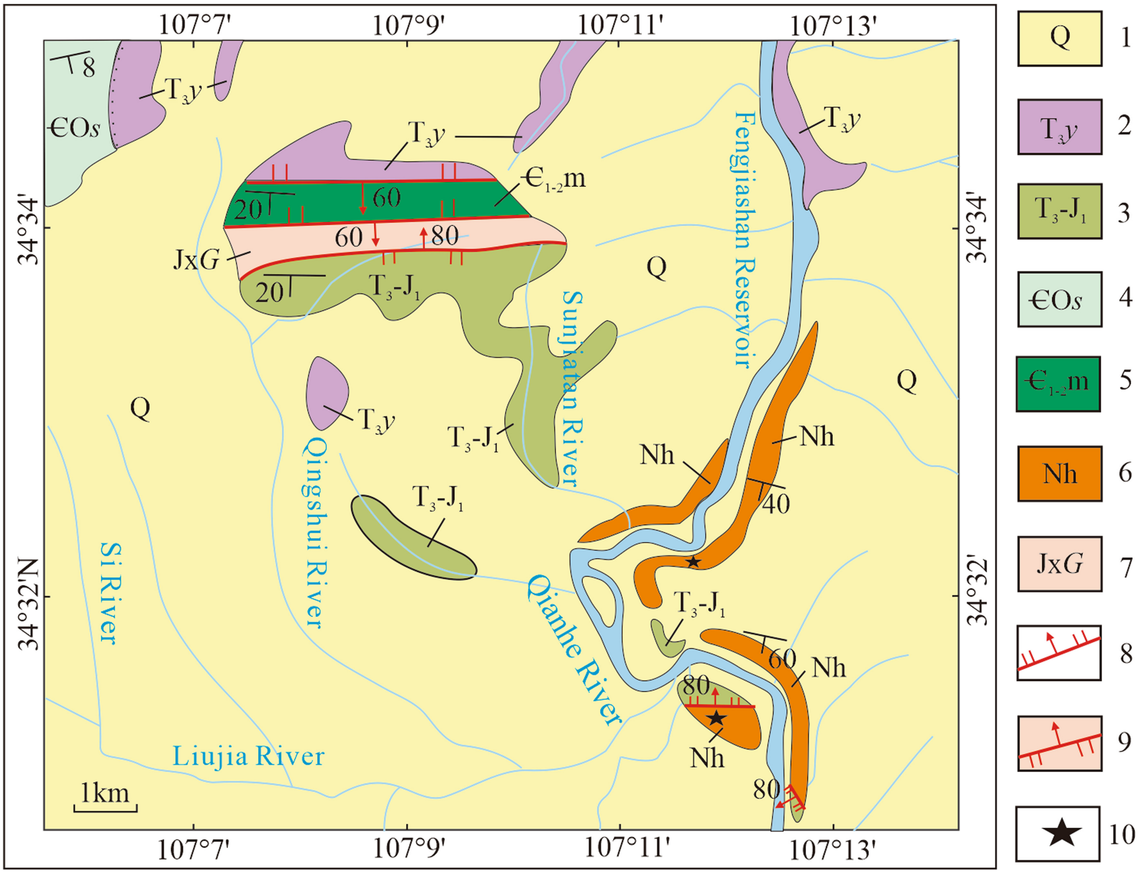

Fig. 3 Geological map of the Changqing low-grade metamorphic clastic rock-carbonate outcrop area in the southern part of Fengjiashan Reservoir (modified after the 1:250,000 geological map of Baoji City, Shaanxi Provincial Geological Survey and Research Institute, 2003. 1:200,000 Baoji Geological Map. The 14th Unit of Qinling Regional Geological Survey Brigade, Shaanxi Provincial Geological Bureau, Ministry of Geology, 1960, and the revision of the results are based on the authors' investigation); 1. Quaternary system; 2. Upper Triassic Yanchang Formation; 3. The Upper Triassic-Lower Jurassic greenschist disintegrated from the original Xiong'er Group; 4. Cambrian-Ordovician Sanshanzi Formation; 5. Lower-Middle Cambrian Mantou Formation; 6. the low-graded metamorphic clastic rock-carbonate of Neoproterozoic Nanhua System disintegrated from the original Xiong'er Group; 7. Guandaokou Group of the Jixian System of Neoproterozoic;8. normal fault; 9. reverse fault; 10. Sampling point

State Key Laboratory of Continental Dynamics, Northwestern University, Xi'an.

For the zircon CL image, the CL luminometer used a CL probe loaded on a scanning electron microscope, Mono CL3 + from Gatan, UK. U–Pb isotopic composition of zircon was tested using quadrupole ICP-MS Elan6100DRC. The laser beam used in the analysis has a spot diameter of 30 µm, a laser pulse of 10 Hz, and an energy of 32–36 mJ. In the analysis of age data, if the measuring point is < 1000 Ma, the $^{206}Pb/^{238}U$ age value is used; if the measuring point is > 1000 Ma, the $^{207}Pb/^{206}Pb$ age value is used instead. The concordance of the data at each measurement point of detrital zircon was calculated in combination with $^{206}Pb/^{238}U$, and the measurement point data whose age deviation between $^{206}Pb/^{238}U$ and $^{207}Pb/^{206}Pb$ was greater than ± 10% were eliminated.

4 Analysis results

Two sandstone samples and one quartzite sample are used for detrital zircon U–Pb LA-ICP-MS dating. The dating analysis data are listed in Tables 1 and 2. For the ancient zircons with age > 1000 Ma, most of them have a certain degree of Pb-loss. The initial conditions of ^{206}Pb and ^{207}Pb are the same and the later geological environment has characteristics of synchronous changes. The ratio and the age of $^{207}Pb/^{206}Pb$ are relatively stable. Therefore, due to its credibility (Diwu et al. 2010), the age results of $^{207}Pb/^{206}Pb$ were used for this study. For the data of zircon aged < 1000 Ma, due to the low content of radioactive Pb that can be used and the uncertainty in the correction of ordinary Pb, the more reliable surface age of $^{206}Pb/^{238}U$ was selected.

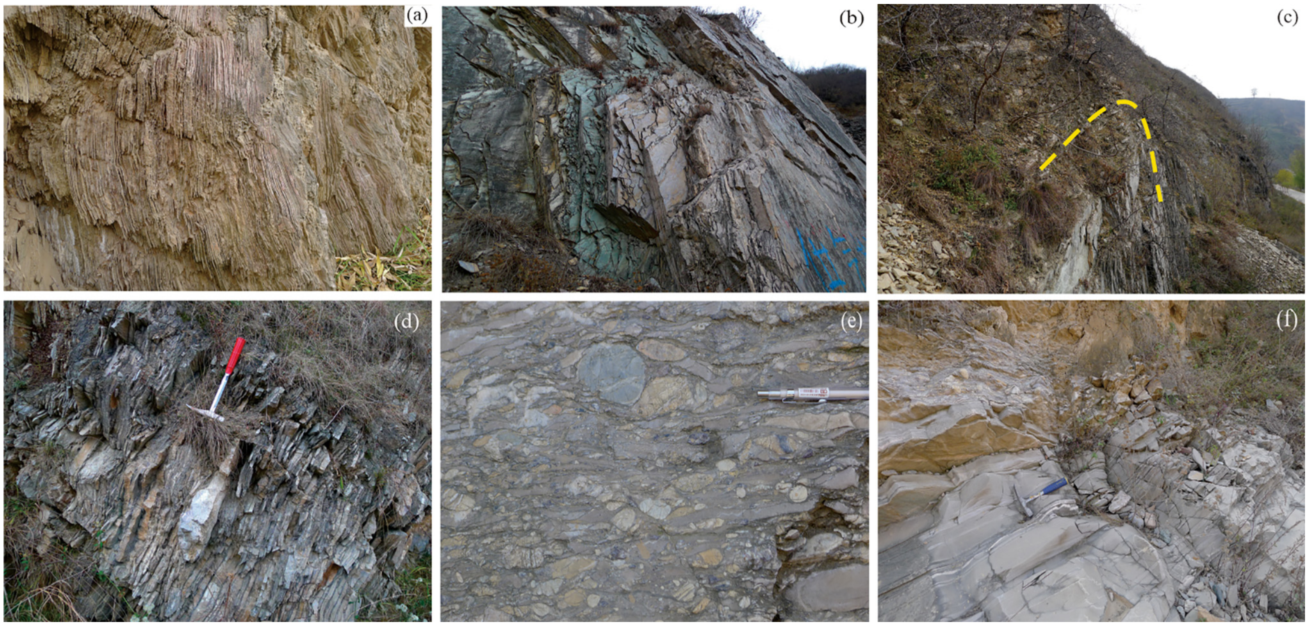

Fig. 4 Photograph of the outcrop of the low-grade metamorphic clastic rock-carbonate in the southern part of Fengjiashan Reservoir **a**, **b** Calcareous slate on the east bank of the Qianhe River; **c** Anticline structure in the calcareous slate on the east bank of the Qianhe River; **d** Thin marbled limestone on the west bank of the Qianhe River; **e** Conglomerate interlayer on the west bank of the Qianhe River; **f** Sandstone interlayer on the west bank of the Qianhe River

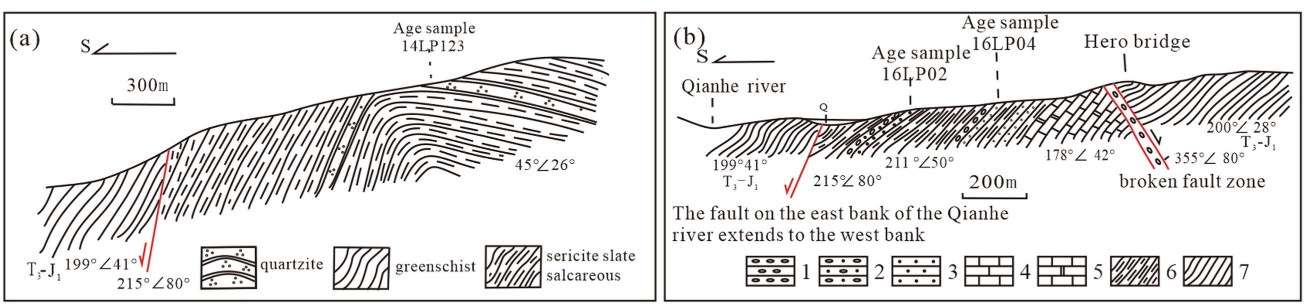

Fig. 5 Geological section along the banks of the Qian River in the southern part of Fengjiashan Reservoir; 1. conglomerate; 2. glutenite; 3. sandstone; 4. limestone; 5. marbled limestone; 6. sericite, calcareous slate; 7. Greenschist. The age sample 14LP01 in the picture is the Youjia (2016) dating sample

4.1 Detrital zircon U–Pb age of quartzite interlayer

In the sericite slate on the eastern bank of the Qianhe River, there are several layers of thin quartzite interlayers, each of which is about 2 to 3 cm thick, and locally formed into small clumps. The dating samples for this research were collected from small clumps of quartzite (Fig. 5a), sampling point coordinates are 34°31′6.9″N, 107°12′9.2″E, and the sample number is 14LP123.

The CL image of detrital zircon in quartzite is shown in Fig. 7a. Zircon particles vary in size and mostly occur in the shape of long columns, containing a small amount of elliptical or round particles, with a particle size between 25 and 110 μm. A small number of particles have better self-shape and roundness, indicating that these zircons have undergone long-distance transportation and sorting, and are detrital in nature. A few particles in the sample developed oscillating belts, and the brightness of the zircons was uneven, where some were darker, which may be due to the higher content of Th and U. Th/U ratio of zircons was 0.18–1.78 (average 0.64), of which only four zircons had ratios less than 0.3. A higher Th/U ratio (> 0.01) indicates most of the samples were of magmatic origin. Eighty zircons in the sample were analyzed, and the effective measuring points were 77 after calibration. These points were all located on the concordance line of the $^{207}Pb/^{235}U$—$^{206}Pb/^{238}U$ concordant diagram, or distributed near it (Fig. 8a), indicating that radiogenic Pb of zircon was not significantly lost, and the dating data is highly reliable. The age of $^{206}Pb/^{238}U$ was between 753 ± 11 Ma

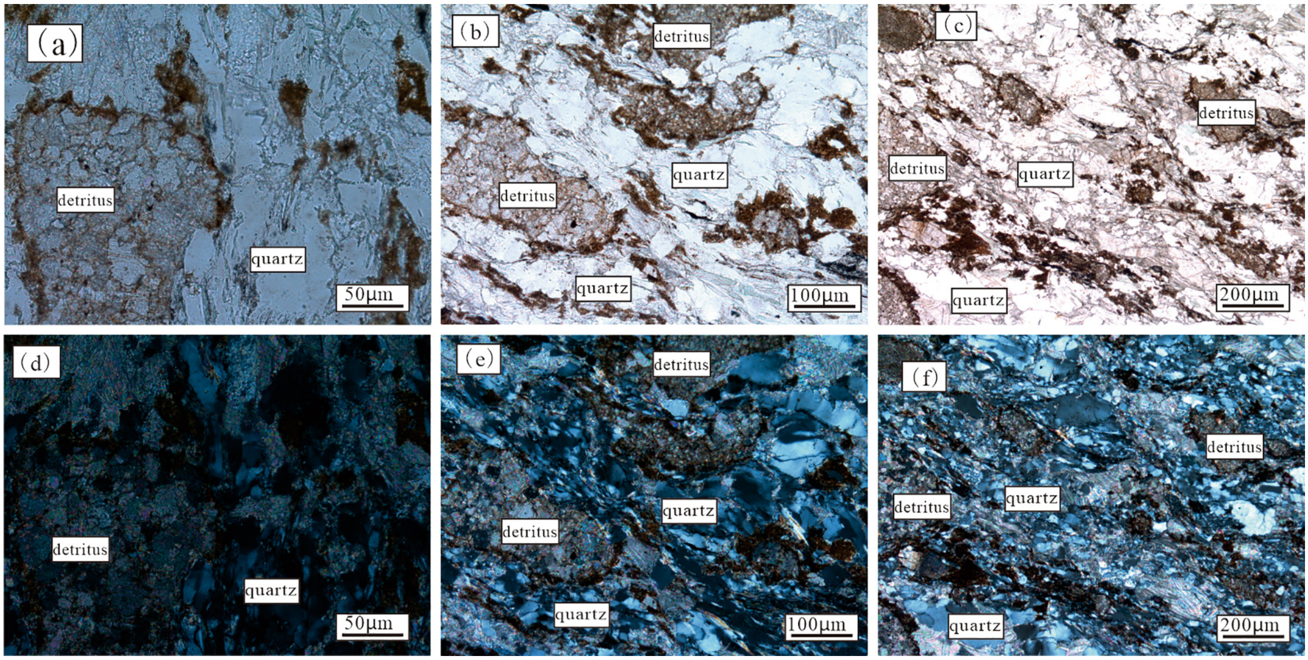

Fig. 6 Photomicrograph of variable sandstone of the low-graded metamorphic clastic rock on the south side of Fengjiashan Reservoir. **a**, **b** and **c** are single polarized lights; Figures **d**, **e**, and **f** are orthogonally polarized lights corresponding to **a**, **b**, and **c**

and 2708 ± 22 Ma, while the age of $^{207}Pb/^{235}U$ was between 907 ± 26 Ma and 2715 ± 22 Ma. A good concordance was observed in $^{206}Pb/^{238}U$ and $^{207}Pb/^{235}U$ (Table 1). The zircon age histogram (Fig. 8b) shows five age peaks (755, 1176, 1500, 1855–2030, and 2259–2418 Ma).

4.2 The U–Pb age of the detrital zircon of sandstone

The sampling point of the low-grade metamorphic sandstone sample (16LP02) was 34°30′57.6″N, 107°12′4.0″E, and the CL image of the detrital zircon in the sample is shown in Fig. 7b. The particle size of zircon is between 40 and 120 μm, most of which are in short or long columns, oblong or round, and have good self-shape and roundness, indicating long-distance transportation and separation. Few zircons developed oscillating zoning, with a majority having no ring or fuzzy rings. Core mantle edge structure could be observed in some particles. Mostly, the brightness of zircon grains was uneven, while the darker ones could be due to the higher content of Th and U. The Th/U ratio of zircon was 0.22–2.32 (average 0.73), which is greater than 0.1. A higher Th/U ratio (> 0.01) indicated that the zircon is of magmatic origin. Out of the 71 zircons analyzed in the sample, the effective measuring points were 60 after calibration, located on or near the concordance line of $^{207}Pb/^{235}U$—$^{206}Pb/^{238}U$ harmony diagram (Fig. 8c), indicating that radiogenic Pb of zircon was not significantly lost, and the dating data is highly reliable. The age of $^{206}Pb/^{238}U$ was between 854 ± 12 Ma and 2507 ± 19 Ma, and the age of $^{207}Pb/^{235}U$ was between 883 ± 17 Ma and 2472 ± 10 Ma, indicating that $^{206}Pb/^{238}U$ and $^{207}Pb/^{235}U$ had a good degree of concordance (Table 2). The age histogram of zircon (Fig. 8d) shows that the sample has five age peaks (858, 1324–1393, 1578, 1912, and 2441 Ma).

4.3 U–Pb ages of detrital zircons of sandstone 16LP04

Another low-grade metamorphic sandstone sample (16LP04) used in the detrital zircon U–Pb dating lay in coordinates 34°31′3.9″N, 107°12′7.6″E (Fig. 5b). The CL image of detrital zircon is shown in Fig. 7c. The particle size of zircon was between 40 and 120 μm, the shape, structure, and brightness of the grains are similar to those observed in sample 16LP02. The Th/U ratio of zircon was 0.24–1.47 (average 0.74), which is greater than 0.1. A higher Th/U ratio (> 0.01) indicates that the zircons in the sample are all magmatic. Out of the 72 particles analyzed, the effective measuring points were 64 after calibration, located on or near the harmony line of $^{207}Pb/^{235}U$—$^{206}Pb/^{238}U$ harmony diagram (Fig. 8e), indicating that the radiogenic Pb of zircon had no obvious loss, and the dating data is highly reliable. The age of $^{206}Pb/^{238}U$ was between 1444 ± 11 and 2735 ± 18 Ma, and the age of $^{207}Pb/^{235}U$ was between 883 ± 17 and 2472 ± 10 Ma, indicating that $^{206}Pb/^{238}U$ and $^{207}Pb/^{235}U$ had a good

Table 1 LA-ICP-MS U-Th-Pb isotope analysis results of detrital zircon in Changqing quartzite (sample number 14LP123)

Station	Pb^* ($\times 10^{-6}$)	^{232}Th ($\times 10^{-6}$)	^{238}U ($\times 10^{-6}$)	Th/U	Isotope ratio						age/Ma					
					$^{207}Pb/^{206}Pb$		$^{207}Pb/^{235}U$		$^{206}Pb/^{238}U$		$^{207}Pb/^{206}Pb$		$^{207}Pb/^{235}U$		$^{206}Pb/^{238}U$	
					Ratio	1σ	Ratio	1σ	Ratio	1σ	Age	1σ	Age	1σ	Age	1σ
1	52.1	209	209	1.00	0.0911	0.0023	2.3306	0.0382	0.1857	0.0020	1172	75	1112	24	1082	12
2	117	404	567	0.71	0.1649	0.0036	3.1623	0.0367	0.1391	0.0014	1746	64	1076	21	776	8
3	12.5	19.1	48.7	0.39	0.0920	0.0031	2.7594	0.0788	0.2175	0.0031	1468	33	1345	21	1269	16
4	80.6	67.3	183	0.37	0.1251	0.0028	6.3186	0.0828	0.3663	0.0038	2030	11	2021	11	2012	18
5	48.9	106	205	0.51	0.0833	0.0021	2.2506	0.0398	0.1960	0.0021	1213	56	1172	18	1150	12
7	9.92	35.6	41.0	0.87	0.0903	0.0041	2.2039	0.0893	0.1771	0.0030	1193	142	1089	45	1038	18
8	49.1	97.0	195	0.50	0.0874	0.0022	2.6489	0.0441	0.2198	0.0023	1318	52	1292	17	1277	13
9	114.9	241	404	0.60	0.0937	0.0022	3.0596	0.0425	0.2367	0.0024	1503	13	1423	11	1370	13
10	30.7	44.6	152	0.29	0.0782	0.0021	1.8976	0.0366	0.1761	0.0019	1028	56	1036	16	1039	11
12	74.3	80.6	437	0.18	0.0800	0.0022	1.9713	0.0396	0.1788	0.0020	1196	22	1106	14	1060	11
13	138	124	299	0.42	0.1290	0.0028	6.7210	0.0797	0.3780	0.0038	2084	9	2075	10	2067	18
14	12.3	18.9	51.9	0.36	0.0823	0.0028	2.2690	0.0632	0.2000	0.0027	1132	78	1156	25	1169	14
15	79.6	99.5	344	0.29	0.0799	0.0019	2.2438	0.0318	0.2037	0.0020	1195	14	1195	10	1195	11
16	149	127	215	0.59	0.1876	0.0041	13.5025	0.1540	0.5221	0.0052	2721	8	2715	11	2708	22
17	83.8	170	360	0.47	0.0847	0.0020	2.4371	0.0376	0.2086	0.0022	1309	15	1254	11	1222	11
18	31.6	68.8	75.3	0.91	0.1117	0.0031	4.8905	0.1045	0.3175	0.0041	1751	70	1760	29	1768	22
19	142	771	762	1.01	0.1391	0.0031	2.5557	0.0311	0.1332	0.0013	2217	10	1288	9	806	7
20	78.2	102	131	0.78	0.1557	0.0035	9.6664	0.1285	0.4502	0.0048	2410	10	2404	12	2396	21
21	55.2	47.1	127	0.37	0.1252	0.0030	6.3232	0.0949	0.3664	0.0040	2031	13	2022	13	2012	19
22	67.8	60.5	126	0.48	0.1694	0.0043	11.2352	0.2034	0.4809	0.0063	2552	15	2543	17	2531	28
23	127	326	401	0.81	0.0956	0.0022	3.3146	0.0480	0.2513	0.0026	1486	53	1459	20	1441	14
24	67.1	132	226	0.59	0.1006	0.0027	3.9321	0.0758	0.2836	0.0033	1634	19	1620	16	1610	17
25	36.3	44.5	68.7	0.65	0.1416	0.0035	8.0285	0.1314	0.4112	0.0048	2247	14	2234	15	2220	22
26	60.1	154	160	0.96	0.1221	0.0030	4.9331	0.0835	0.2930	0.0033	1988	15	1808	14	1656	17
27	34.4	69.7	62.3	1.12	0.1382	0.0038	7.5427	0.1555	0.3959	0.0053	2205	18	2178	18	2150	25
28	26.8	46.7	63.4	0.74	0.1136	0.0032	5.1814	0.1092	0.3307	0.0043	1858	20	1850	18	1842	21
29	14.6	32.4	34.1	0.95	0.1130	0.0044	4.9344	0.1716	0.3167	0.0058	1744	112	1753	47	1760	31
30	104	126	484	0.26	0.0790	0.0018	2.0803	0.0275	0.1911	0.0019	1171	12	1142	9	1127	10
31	37.8	53.2	61.6	0.86	0.1598	0.0041	10.1259	0.1852	0.4596	0.0060	2453	15	2446	17	2438	26
32	31.1	99.3	163	0.61	0.0931	0.0026	2.8145	0.0586	0.2193	0.0026	1387	66	1315	23	1271	14
33	63.5	120	199	0.60	0.1012	0.0026	3.9058	0.0677	0.2800	0.0031	1579	54	1582	20	1585	16
34	43.4	89.9	85.0	1.06	0.1271	0.0031	6.3970	0.1061	0.3652	0.0042	2058	14	2032	15	2007	20
35	8.45	9.86	52.1	0.19	0.1271	0.0045	2.2803	0.0670	0.1301	0.0019	1461	96	957	29	753	11

Table 1 continued

Station	Pb^{*} ($\times 10^{-6}$)	^{232}Th ($\times 10^{-6}$)	^{238}U ($\times 10^{-6}$)	Th/U	Isotope ratio						age/Ma					
					$^{207}Pb/^{206}Pb$		$^{207}Pb/^{235}U$		$^{206}Pb/^{238}U$		$^{207}Pb/^{206}Pb$		$^{207}Pb/^{235}U$		$^{206}Pb/^{238}U$	
					Ratio	1σ	Ratio	1σ	Ratio	1σ	Age	1σ	Age	1σ	Age	1σ
36	79.5	233	265	0.88	0.0957	0.0024	3.2859	0.0561	0.2490	0.0027	1542	17	1478	13	1433	14
37	65.9	123	219	0.56	0.0921	0.0022	3.2375	0.0473	0.2549	0.0026	1470	14	1466	11	1463	13
38	41.0	48.9	74.2	0.66	0.1570	0.0038	9.7671	0.1576	0.4512	0.0054	2424	13	2413	15	2400	24
39	50.5	72.7	114	0.64	0.1215	0.0030	5.8718	0.0955	0.3505	0.0040	1892	49	1908	20	1924	20
40	94.1	244	319	0.77	0.0991	0.0024	3.6960	0.0557	0.2705	0.0028	1607	14	1571	12	1543	14
41	119	269	527	0.51	0.0851	0.0020	2.3224	0.0323	0.1979	0.0020	1318	13	1219	10	1164	11
42	10.6	17.1	42.3	0.40	0.1099	0.0039	2.9410	0.0891	0.1940	0.0029	1163	115	1121	37	1100	16
43	59.7	267	202	1.32	0.0820	0.0020	2.3032	0.0378	0.2037	0.0021	1246	17	1213	12	1195	11
44	117	237	253	0.94	0.1188	0.0028	5.6351	0.0877	0.3440	0.0038	1938	14	1921	13	1906	18
45	79.4	281	405	0.70	0.0931	0.0026	3.0768	0.0654	0.2398	0.0029	1489	23	1427	16	1386	15
46	23.8	44.6	107	0.42	0.0806	0.0024	2.1951	0.0516	0.1975	0.0024	1212	27	1179	16	1162	13
47	6.14	11.8	21.0	0.52	0.0883	0.0040	2.6816	0.1103	0.2203	0.0039	1294	115	1283	40	1277	21
48	46.5	50.8	87.7	0.58	0.1454	0.0035	8.4339	0.1364	0.4208	0.0050	2292	13	2279	15	2264	22
49	60.2	243	358	0.68	0.0858	0.0021	1.6941	0.0271	0.1433	0.0015	1333	16	1006	10	863	8
50	54.1	112	188	0.60	0.0857	0.0021	2.7391	0.0436	0.2318	0.0024	1332	16	1339	12	1344	13
51	58.7	56.3	273	0.21	0.0792	0.0020	2.1034	0.0353	0.1927	0.0020	1177	17	1150	12	1136	11
52	60.1	64.3	113	0.57	0.1833	0.0047	12.6271	0.2419	0.4997	0.0070	2683	15	2652	18	2612	30
53	64.6	173	263	0.66	0.0810	0.0020	2.2348	0.0364	0.2001	0.0021	1221	17	1192	11	1176	11
54	22.9	60.3	89.00	0.68	0.0828	0.0024	2.3372	0.0522	0.2046	0.0024	1265	25	1224	16	1200	13
55	64.1	123	220	0.56	0.0905	0.0022	3.0021	0.0468	0.2407	0.0025	1435	15	1408	12	1390	13
56	20.5	72.4	40.6	1.78	0.1128	0.0035	5.0249	0.1253	0.3230	0.0046	1845	25	1824	21	1804	22
57	41.8	85.8	112	0.77	0.1022	0.0025	4.0247	0.0671	0.2857	0.0031	1664	16	1639	14	1620	16
58	64.1	121	293	0.41	0.0791	0.0019	2.1439	0.0346	0.1967	0.0020	1173	17	1163	11	1158	11
59	65.8	62.3	136	0.46	0.1276	0.0029	6.5396	0.0892	0.3718	0.0039	2065	11	2051	12	2038	18
60	48.0	83.8	142	0.59	0.1033	0.0026	4.1437	0.0732	0.2910	0.0033	1684	17	1663	14	1647	16
61	55.7	94.6	214	0.44	0.0966	0.0025	3.0514	0.0546	0.2291	0.0025	1477	52	1383	18	1323	14
62	123	581	641	0.91	0.0851	0.0020	1.7315	0.0251	0.1475	0.0015	1319	14	1020	9	887	8
63	164	470	129	0.36	0.1578	0.0037	3.0128	0.0423	0.1384	0.0014	1289	91	907	26	758	8
64	65.4	68.3	247	0.28	0.0882	0.0021	2.8387	0.0416	0.2335	0.0024	1387	14	1366	11	1353	12
65	73.7	163	338	0.48	0.0861	0.0025	2.3113	0.0502	0.1947	0.0023	1204	67	1161	21	1139	13
66	26.2	61.5	75.9	0.81	0.0972	0.0027	3.5523	0.0728	0.2651	0.0032	1571	21	1539	16	1516	16
67	59.09	69.4	165	0.42	0.1097	0.0026	4.7432	0.0738	0.3135	0.0034	1795	14	1775	13	1758	17
68	5.83	10.4	28.0	0.37	0.0774	0.0038	2.0184	0.0908	0.1890	0.0033	1133	61	1122	31	1116	18

Table 1 continued

Station	Pb^* ($\times 10^{-6}$)	^{232}Th ($\times 10^{-6}$)	^{238}U ($\times 10^{-6}$)	Th/U	Isotope ratio						age/Ma					
					$^{207}Pb/^{206}Pb$		$^{207}Pb/^{235}U$		$^{206}Pb/^{238}U$		$^{207}Pb/^{206}Pb$		$^{207}Pb/^{235}U$		$^{206}Pb/^{238}U$	
					Ratio	1σ	Ratio	1σ	Ratio	1σ	Age	1σ	Age	1σ	Age	1σ
69	44.2	78.9	84.5	0.93	0.1113	0.0038	4.5934	0.1277	0.2994	0.0046	1712	93	1692	38	1675	25
70	64.5	307	231	1.33	0.0933	0.0024	2.8795	0.0502	0.2238	0.0024	1495	17	1377	13	1302	13
71	32.2	70.7	102	0.69	0.0908	0.0024	3.0933	0.0576	0.2470	0.0028	1443	19	1431	14	1423	14
72	41.0	53.3	78.7	0.68	0.1538	0.0037	9.4438	0.1548	0.4454	0.0054	2388	13	2382	15	2375	24
73	39.4	51.2	85.6	0.60	0.1212	0.0031	5.9165	0.1054	0.3541	0.0042	1974	16	1964	15	1954	20
74	83.5	52.7	221	0.24	0.1161	0.0026	5.3546	0.0741	0.3344	0.0035	1897	12	1878	12	1860	17
75	45.4	118	193	0.61	0.0833	0.0023	2.3622	0.0470	0.2057	0.0023	1276	22	1231	14	1206	12
77	47.0	57.8	144	0.40	0.1038	0.0026	4.1804	0.0735	0.2921	0.0033	1693	17	1670	14	1652	17
78	17.6	29.1	25.8	1.13	0.1587	0.0044	10.0497	0.2223	0.4592	0.0067	2442	19	2439	20	2436	30
79	47.8	86.7	143	0.60	0.1046	0.0026	4.1727	0.0687	0.2892	0.0032	1626	52	1628	20	1629	17
80	64.4	122.1	204	0.60	0.1131	0.0032	4.8995	0.1100	0.3142	0.0042	1849	22	1802	19	1762	21

degree of concordance (Table 2). The zircon age histogram (Fig. 8f) shows that the sample has five age peaks (1318, 1586, 1822–1949, 2207–2316, and 2482–2532 Ma).

5 Discussion

Detrital zircon U–Pb dating results of the Changqing low-grade clastic metamorphic rocks can indirectly limit the deposition time of this set of strata and provide new evidence for the stratum attribution. The detrital zircon age lineage of the rocks had good correspondence with the Neoarchean-Paleoproterozoic geological evolution of the NCC. The age spectrum was very similar to that of the Ordos basement before cratonization ($\sim$ 1.9–1.8 Ga) of the NCC, but great differences existed after cratonization.

5.1 Formation age and stratum attribution

The detrital zircon U–Pb dating results of the Changqing low-grade metamorphic sandstone and quartzite on the southern side of Fengjiashan Reservoir showed that the concordant age ranged from 753 to 2735 Ma. If the U–Pb system is not disturbed and the sample is not contaminated, the youngest age data obtained from the detrital zircon in the sedimentary rock sample would provide the maximum sedimentation age of the sediment (Nelson 2001). The minimum age was 753 Ma, with multiple measuring points near 753 Ma, indicating that it is not a coincidence, rather, the deposition age of low-grade metamorphic strata should be younger than 753 Ma. You (2016) analyzed the zircon U–Pb dating of the residual detrital sandstone to obtain an age of 1091 $\pm$ 46 to 2854 $\pm$ 170 Ma, indicating that the formation time of the low-grade clastic metamorphic rock-carbonate should not be earlier than 1091 Ma.

According to the stratigraphic contact relationship, the formation age of the Changqing low-grade clastic metamorphic rock-carbonate cannot be directly defined. Field observations showed that these rocks are in contact with the Changqing greenschist through normal faults, while the Guandaokou Group argillaceous limestone is overlaid on the greenschist in the southwestern part of Fengjiashan Reservoir. Considering that in the Miaopoli section of Qishan County, the Neoproterozoic Sinian Luoquan Formation is covered by parallel unconformities on the Guandaokou Group, and the Luoquan Formation is covered by platform facies Cambrian-Ordovician strata with parallel unconformities. Because the Fengjiashan Reservoir is not far from the Qishan Miaopoli section (about 41 km apart), it is inferred that the deposition time of the Low-grade clastic metamorphic rock-carbonate should be after 753 Ma and before Sinian. This period corresponds to the new Proterozoic Stretching Period or Nanhua Period.

Table 2 LA-ICP-MS U-Th-Pb isotope analysis results of detrital zircon in the Changqing low-grade metamorphic quartz sandstone (sample numbers 16LP02, 16LP04)

Station	Pb^{*} ($\times 10^{-6}$)	^{232}Th ($\times 10^{-6}$)	^{238}U ($\times 10^{-6}$)	Th/U	Isotope ratio						age (Ma)					
					$^{207}Pb/^{206}Pb$		$^{207}Pb/^{235}U$		$^{206}Pb/^{238}U$		$^{207}Pb/^{206}Pb$		$^{207}Pb/^{235}U$		$^{206}Pb/^{238}U$	
					Ratio	1σ	Ratio	1σ	Ratio	1σ	Age	1σ	Age	1σ	Age	1σ
16LP02 (Metamorphic lithic sandstone)																
1	70.3	95.2	136	0.70	0.1377	0.0019	7.7459	0.0772	0.4081	0.0034	2198	8	2202	9	2206	16
2	83.8	64.2	195	0.33	0.1209	0.00159	6.2179	0.0572	0.3729	0.0026	1970	7	2007	8	2043	13
3	50.7	113	173	0.65	0.0853	0.0013	2.8348	0.0333	0.2410	0.0020	1323	11	1365	9	1392	10
4	12.2	24.2	26.3	0.92	0.1192	0.0030	5.6650	0.1224	0.3446	0.0052	1945	19	1926	19	1909	25
5	109	107	275	0.39	0.1191	0.0016	5.5314	0.0556	0.3369	0.0027	1910	28	1887	11	1867	13
6	11.7	22.0	26.1	0.84	0.1107	0.0032	5.2791	0.1306	0.3459	0.0058	1811	23	1865	21	1915	28
7	61.8	99.7	137	0.73	0.1096	0.0016	5.4278	0.0585	0.3592	0.0030	1793	9	1889	9	1978	14
8	23.4	37.7	54.0	0.70	0.1219	0.0025	5.6955	0.0959	0.3390	0.0041	1860	54	1862	22	1863	21
10	43.4	94.7	87.6	1.08	0.1242	0.0020	6.1735	0.0758	0.3606	0.0034	2017	10	2001	11	1985	16
11	67.8	74.3	111	0.67	0.1599	0.0021	10.3820	0.1007	0.4709	0.0040	2455	7	2469	9	2488	17
12	23.1	42.0	50.9	0.83	0.1101	0.0021	5.2946	0.0834	0.3488	0.0039	1801	14	1868	13	1929	19
13	41.8	89	93.4	0.96	0.1139	0.0019	5.2197	0.0712	0.3323	0.0033	1863	12	1856	12	1849	16
17	71.7	86.4	136	0.64	0.1394	0.0021	7.8254	0.0897	0.4071	0.0038	2220	9	2211	10	2202	17
18	58.7	41.1	130	0.32	0.1236	0.0016	6.5563	0.0640	0.3848	0.0031	2008	8	2053	9	2099	14
20	20.6	16.3	35.5	0.46	0.1571	0.0028	10.0450	0.1420	0.4637	0.0053	2425	11	2439	13	2456	23
21	49.1	45.6	81.3	0.56	0.1589	0.0023	10.3942	0.1107	0.4745	0.0043	2444	8	2471	10	2503	19
22	10.5	22.1	21.4	1.03	0.1173	0.0033	5.7785	0.1385	0.3571	0.0059	1916	21	1943	21	1969	28
23	58.8	153	139	1.10	0.0977	0.0014	4.1506	0.0466	0.3081	0.0026	1581	10	1664	9	1731	13
25	37.6	98.6	99.4	0.99	0.0973	0.0017	3.7778	0.0517	0.2814	0.0027	1574	13	1588	11	1599	13
26	36.6	37.9	83.4	0.45	0.1169	0.0019	5.9008	0.0734	0.3660	0.0034	1910	11	1961	11	2011	16
27	86.9	201	161	1.25	0.1166	0.0016	6.0724	0.0628	0.3776	0.00309	1905	9	1986	9	2065	14
29	40.4	130	90.7	1.43	0.1427	0.0023	5.3118	0.0640	0.2700	0.0026	2260	10	1871	10	1541	13
30	8.96	16.8	20.0	0.84	0.1160	0.00320	5.3635	0.1275	0.3354	0.0054	1895	21	1879	20	1864	26
32	63.4	64.8	148	0.44	0.11640	0.00160	5.7188	0.0597	0.3562	0.0029	1902	9	1934	9	1964	14
33	13.6	73.2	70.9	1.03	0.07090	0.0023	1.3854	0.0392	0.1416	0.0021	956	34	883	17	854	12
34	60.1	93.8	138	0.68	0.1199	0.0016	5.6124	0.0565	0.3394	0.0027	1915	32	1895	13	1878	14
35	25.2	56.2	58.8	0.96	0.1116	0.0020	4.9029	0.0712	0.3185	0.0033	1826	13	1803	12	1782	16
36	65.6	268	115	2.32	0.1044	0.0018	4.6977	0.0652	0.3262	0.0032	1704	12	1767	12	1820	16
37	57.0	67.7	90.3	0.75	0.1561	0.0022	10.2189	0.1041	0.4748	0.0041	2414	8	2455	9	2504	18
38	69.1	99.3	127	0.78	0.1325	0.0018	7.5635	0.0733	0.4140	0.0033	2131	8	2181	9	2233	15
39	54.1	86.5	100	0.86	0.1264	0.0018	7.0236	0.0733	0.4030	0.0034	2048	8	2114	9	2183	15
40	30.5	47.7	67.5	0.71	0.1103	0.0020	5.3538	0.0798	0.3521	0.0037	1804	13	1878	13	1945	18

Acta Geochim (2023) 42:912–933

Table 2 continued

Station	Pb* ($\times 10^{-6}$)	^{232}Th ($\times 10^{-6}$)	^{238}U ($\times 10^{-6}$)	Th/U	Isotope ratio						age (Ma)					
					^{207}Pb/^{206}Pb		^{207}Pb/^{235}U		^{206}Pb/^{238}U		^{207}Pb/^{206}Pb		^{207}Pb/^{235}U		^{206}Pb/^{238}U	
					Ratio	1σ	Ratio	1σ	Ratio	1σ	Age	1σ	Age	1σ	Age	1σ
41	44.7	57.1	69.1	0.83	0.1584	0.0023	10.2244	0.1087	0.4680	0.0042	2439	8	2455	10	2475	18
42	32.9	37.8	54.3	0.70	0.1579	0.0024	9.9964	0.1167	0.4590	0.0045	2434	9	2434	11	2435	20
43	42.7	32.8	109	0.30	0.1204	0.0019	5.5253	0.0681	0.3329	0.0031	1962	10	1905	11	1852	15
44	33.5	90.5	73.68	1.23	0.1087	0.0018	4.7697	0.0616	0.3182	0.0030	1777	11	1780	11	1781	15
45	27.3	30.3	62.07	0.49	0.1178	0.0021	5.7933	0.0848	0.3567	0.0038	1923	13	1945	13	1966	18
46	23.9	32.8	52.72	0.62	0.1175	0.0025	5.7911	0.0999	0.3574	0.0044	1919	15	1945	15	1970	21
49	112	124	324	0.38	0.1134	0.0014	4.4743	0.0386	0.2860	0.0020	1770	25	1681	9	1611	10
50	105	89.4	201	0.44	0.1494	0.0020	8.5355	0.0801	0.4142	0.0033	2282	26	2253	11	2221	16
51	47.3	33.1	81.4	0.41	0.1602	0.0022	10.1692	0.1048	0.4603	0.0040	2458	8	2450	10	2441	18
52	34.1	48.8	57.6	0.85	0.1629	0.0026	9.4056	0.1139	0.4186	0.0042	2324	40	2271	18	2213	21
53	12.2	20.1	26.5	0.76	0.1158	0.0029	5.5492	0.1157	0.3476	0.0050	1892	19	1908	18	1923	24
54	107	90.6	197	0.46	0.1461	0.0018	8.7609	0.0738	0.4349	0.0032	2301	6	2313	8	2328	14
55	32.9	50.9	112	0.45	0.0883	0.0015	2.9420	0.0404	0.2416	0.0022	1389	13	1393	10	1395	11
56	22.8	37.3	48.1	0.78	0.1205	0.0022	5.9218	0.0887	0.3564	0.0040	1964	13	1964	13	1965	19
58	68.4	54.8	156	0.35	0.1176	0.0016	5.9162	0.0573	0.3649	0.0028	1919	8	1964	8	2005	13
59	46.1	40.8	89.5	0.46	0.1328	0.0020	7.5628	0.0888	0.4129	0.0038	2136	9	2180	11	2228	17
60	8.19	17.8	17.7	1.01	0.1140	0.0038	5.2441	0.1518	0.3336	0.0064	1864	26	1860	25	1856	31
61	90.4	93.2	182	0.51	0.1464	0.0019	7.5262	0.072	0.3728	0.0030	2058	32	2026	13	1995	15
62	38.5	41.2	83.6	0.49	0.1277	0.0019	6.3997	0.0728	0.3634	0.0032	2005	32	1996	13	1988	16
63	31.5	68.2	59.8	1.14	0.1166	0.0023	5.8394	0.0930	0.3631	0.0041	1905	14	1952	14	1997	20
64	25.5	41.1	56.1	0.73	0.1114	0.0021	5.3190	0.0831	0.3462	0.0038	1823	14	1872	13	1916	18
65	69.9	26.3	122	0.22	0.1588	0.0023	10.4090	0.1155	0.4753	0.0044	2443	8	2472	10	2507	19
66	22.6	39.1	51.7	0.75	0.1112	0.0021	5.0765	0.0777	0.3310	0.0036	1820	14	1832	13	1843	17
67	16.6	35.2	42.0	0.84	0.1112	0.0024	4.4112	0.0797	0.2878	0.0036	1596	67	1601	26	1606	19
68	112	153	256	0.60	0.1169	0.0014	5.5103	0.0472	0.3419	0.0024	1909	7	1902	7	1896	12
69	14.9	18.2	27.9	0.65	0.1329	0.0031	7.4071	0.1458	0.4040	0.0058	2137	16	2162	18	2188	27
70	75.6	87.0	145	0.60	0.1291	0.0020	7.1575	0.0847	0.4021	0.0037	2085	10	2131	11	2179	17
71	41.5	45.9	86.5	0.53	0.1278	0.0019	6.6478	0.0761	0.3771	0.0037	2068	9	2066	10	2063	16
16LP04 (Metamorphic lithic sandstone)																
1	35.0	76.1	131	0.58	0.1101	0.0019	5.1738	0.0719	0.3407	0.0034	1802	12	1848	12	1890	16
3	16.8	24.5	23.1	1.06	0.1209	0.0026	6.0085	0.1089	0.3604	0.0047	1970	16	1977	16	1984	22
4	12.3	49.6	48.4	1.02	0.1326	0.0043	6.5777	0.1806	0.3597	0.0071	2133	23	2056	24	1981	33
5	26.4	29.8	40.3	0.74	0.1288	0.0026	6.8071	0.1115	0.3833	0.0046	2082	14	2087	15	2091	22

Table 2 continued

Station	Pb^{*} ($\times 10^{-6}$)	^{232}Th ($\times 10^{-6}$)	^{238}U ($\times 10^{-6}$)	Th/U	Isotope ratio						age (Ma)					
					$^{207}Pb/^{206}Pb$		$^{207}Pb/^{235}U$		$^{206}Pb/^{238}U$		$^{207}Pb/^{206}Pb$		$^{207}Pb/^{235}U$		$^{206}Pb/^{238}U$	
					Ratio	1σ	Ratio	1σ	Ratio	1σ	Age	1σ	Age	1σ	Age	1σ
6	19.0	45.4	47.8	0.95	0.1145	0.0026	5.6275	0.1083	0.3564	0.0047	1872	17	1920	17	1965	23
7	22.1	108	238	0.45	0.1133	0.0022	5.2187	0.0830	0.3341	0.0037	1853	14	1856	14	1858	18
8	103	58.6	75.1	0.78	0.1194	0.0015	5.7376	0.0492	0.3485	0.0025	1947	7	1937	7	1927	12
9	35.1	306	358	0.86	0.1198	0.0020	5.8022	0.0733	0.3513	0.0033	1953	11	1947	11	1941	16
11	23.1	60.8	99.9	0.61	0.1095	0.0025	4.9667	0.0940	0.3290	0.0042	1791	17	1814	16	1833	20
13	19.7	34.9	87.1	0.40	0.1496	0.0028	8.9999	0.1374	0.4364	0.0052	2341	12	2338	14	2334	23
14	46.3	176	242	0.72	0.1391	0.0020	8.1983	0.0871	0.4275	0.0037	2216	8	2253	10	2294	17
15	121	47.2	72.6	0.65	0.1242	0.0015	6.4946	0.0550	0.3792	0.0027	2018	7	2045	7	2073	13
16	35.2	215	407	0.53	0.1257	0.0025	6.4124	0.1029	0.3700	0.0043	2039	14	2034	14	2029	20
18	26.5	32.1	40.3	0.80	0.1584	0.0031	9.9469	0.1572	0.4555	0.0058	2438	12	2430	15	2420	26
19	17.7	86.2	101	0.85	0.1125	0.0024	5.0840	0.0875	0.3277	0.0039	1841	15	1833	15	1827	19
20	46.3	54.5	55.7	0.98	0.1105	0.0018	5.1648	0.0648	0.3389	0.0031	1808	11	1847	11	1881	15
21	27.9	38.1	38.3	0.99	0.1194	0.0024	5.8856	0.0946	0.3574	0.0041	1948	14	1959	14	1970	20
22	19.6	28.6	34.8	0.82	0.1218	0.0026	6.0356	0.1044	0.3594	0.0045	1983	15	1981	15	1979	21
23	15.7	45.6	59.4	0.77	0.1169	0.0027	5.3441	0.1020	0.3317	0.0044	1794	64	1814	26	1831	23
24	26.6	40.3	35.2	1.15	0.1115	0.0020	5.1909	0.0751	0.3375	0.0035	1824	13	1851	12	1875	17
25	18.3	37.1	64.4	0.58	0.1183	0.0028	5.8457	0.1178	0.3585	0.0050	1930	18	1953	17	1975	24
26	28.4	33.8	44.9	0.75	0.1129	0.0022	5.3661	0.0838	0.3448	0.0038	1846	14	1879	13	1910	18
27	27.1	22.2	26.7	0.83	0.1472	0.0024	9.0991	0.1165	0.4484	0.0046	2313	10	2348	12	2388	20
28	13.6	17.5	29.6	0.59	0.1154	0.0026	6.0251	0.1162	0.3785	0.0051	1887	17	1979	17	2069	24
29	13.4	20.3	46.1	0.44	0.1190	0.0036	5.7781	0.1505	0.3523	0.0063	1941	23	1943	23	1946	30
30	20.5	25.3	46.5	0.54	0.1212	0.0031	5.9404	0.1262	0.3556	0.0053	1973	19	1967	18	1961	25
31	20.2	61.7	93.4	0.66	0.1177	0.0023	5.4900	0.0865	0.3384	0.0038	1921	14	1899	14	1879	18
32	67.8	44.5	133	0.33	0.1915	0.0025	13.9498	0.1256	0.5285	0.0043	2755	7	2746	9	2735	18
33	56.7	354	591	0.60	0.1206	0.0017	5.9330	0.0591	0.3567	0.0028	1966	8	1966	9	1967	13
35	41.4	121	268	0.45	0.1113	0.0018	5.0707	0.0652	0.3304	0.0031	1821	11	1831	11	1840	15
36	139	61.0	72.0	0.85	0.1385	0.0016	7.8614	0.0610	0.4117	0.0028	2209	6	2215	7	2223	13
37	35.5	848	577	1.47	0.1176	0.0020	5.8589	0.0783	0.3614	0.00355	1920	11	1955	12	1989	17
39	44.0	39.3	42.6	0.92	0.1139	0.0018	5.3916	0.0645	0.3434	0.0031	1862	10	1884	10	1903	15
40	19.8	42.7	61.7	0.69	0.1115	0.0023	5.1382	0.0895	0.3343	0.0040	1824	16	1842	15	1859	19
41	28.8	703	951	0.74	0.1237	0.0023	5.9383	0.0882	0.3483	0.0038	1886	48	1897	20	1907	19
43	110	65.4	277	0.24	0.1407	0.0017	8.2197	0.0687	0.4238	0.0031	2236	6	2256	8	2278	14
44	152	78.3	131	0.60	0.1572	0.0018	9.9044	0.0769	0.4570	0.0032	2426	6	2426	7	2426	14

Table 2 continued

Station	Pb^* ($\times 10^{-6}$)	^{232}Th ($\times 10^{-6}$)	^{238}U ($\times 10^{-6}$)	Th/U	Isotope ratio						age (Ma)					
					$^{207}Pb/^{206}Pb$		$^{207}Pb/^{235}U$		$^{206}Pb/^{238}U$		$^{207}Pb/^{206}Pb$		$^{207}Pb/^{235}U$		$^{206}Pb/^{238}U$	
					Ratio	1σ	Ratio	1σ	Ratio	1σ	Age	1σ	Age	1σ	Age	1σ
45	41.3	74.1	61.6	1.20	0.0850	0.0014	2.9408	0.0378	0.2512	0.0023	1315	13	1392	10	1444	11
46	33.1	62.3	105	0.59	0.1214	0.0021	6.0802	0.0815	0.3634	0.0036	1976	11	1987	12	1998	17
47	51.5	59.0	54.5	1.08	0.1275	0.0018	6.7066	0.0703	0.3815	0.0032	2064	8	2073	9	2083	15
48	26.1	41.0	40.2	1.02	0.1110	0.0025	5.1129	0.0941	0.3341	0.0042	1816	17	1838	16	1858	20
49	16.2	27.8	86.4	0.32	0.0978	0.0023	3.8851	0.0782	0.2881	0.0037	1583	20	1611	16	1632	19
50	40.2	55.3	130	0.42	0.1261	0.0020	6.6625	0.0809	0.3832	0.0036	2044	10	2068	11	2091	17
51	80.7	102	204	0.50	0.1673	0.0021	11.1652	0.0971	0.4841	0.0037	2531	7	2537	8	2545	16
52	96.4	23.1	26.3	0.88	0.1285	0.0016	6.6253	0.0591	0.3742	0.0028	2077	7	2063	8	2049	13
53	12.2	45.7	59.1	0.77	0.1136	0.0028	5.3390	0.1126	0.3408	0.0049	1858	19	1875	18	1891	23
54	35.7	47.7	103	0.46	0.1466	0.0023	8.9350	0.1075	0.4421	0.0043	2307	9	2331	11	2360	19
55	54.7	36.6	49.9	0.73	0.1376	0.0021	7.9310	0.0898	0.4174	0.0038	2200	9	2223	10	2248	17
56	28.8	42.1	63.2	0.67	0.1386	0.0023	8.1576	0.1065	0.4270	0.0044	2209	10	2249	12	2292	20
57	29.1	31.2	32.2	0.97	0.1139	0.0020	5.5258	0.0777	0.3519	0.0036	1863	12	1905	12	1944	17
58	15.5	34.5	42.6	0.81	0.1154	0.0029	5.4375	0.1147	0.3418	0.0049	1886	19	1891	18	1895	24
59	21.5	129	291	0.44	0.1196	0.0023	6.1207	0.0959	0.3713	0.0042	1950	13	1993	14	2035	20
60	118	63.2	141	0.45	0.1127	0.0014	5.1163	0.0423	0.3294	0.0023	1843	7	1839	7	1836	11
61	61.5	50.2	43.5	1.15	0.1177	0.0017	5.7112	0.0597	0.3521	0.0029	1921	9	1933	9	1945	14
62	24.8	124	146	0.85	0.1301	0.0026	7.0076	0.1143	0.3906	0.0047	2100	14	2112	14	2126	22
64	94.1	141	370	0.38	0.1372	0.0018	7.7807	0.0709	0.4113	0.0031	2193	7	2206	8	2221	14
65	138	35.7	39.2	0.91	0.1191	0.0015	5.0337	0.0445	0.3067	0.0022	1942	7	1825	7	1724	11
66	20.3	60.7	113	0.54	0.1202	0.0024	6.1478	0.1001	0.3711	0.0043	1959	14	1997	14	2035	20
67	47.3	93.1	118	0.79	0.1114	0.0016	5.0700	0.0571	0.3303	0.0028	1822	10	1831	10	1840	14
68	52.4	45.9	36.3	1.26	0.1113	0.0016	5.0738	0.0562	0.3307	0.0028	1821	9	1832	9	1842	13
69	19.2	94.8	86.1	1.10	0.1194	0.0024	5.8412	0.0981	0.3549	0.0042	1947	15	1953	15	1958	20
70	35.8	58.2	111	0.52	0.1095	0.0021	4.7699	0.0725	0.3161	0.00336	1791	14	1780	13	1771	16
71	51.3	42.8	45.4	0.94	0.1197	0.0018	5.9922	0.0670	0.3632	0.0031	1952	9	1975	10	1997	15
72	21.2	38.7	78.2	0.50	0.1117	0.0023	5.1823	0.0873	0.3367	0.00394	1826	15	1850	14	1871	19

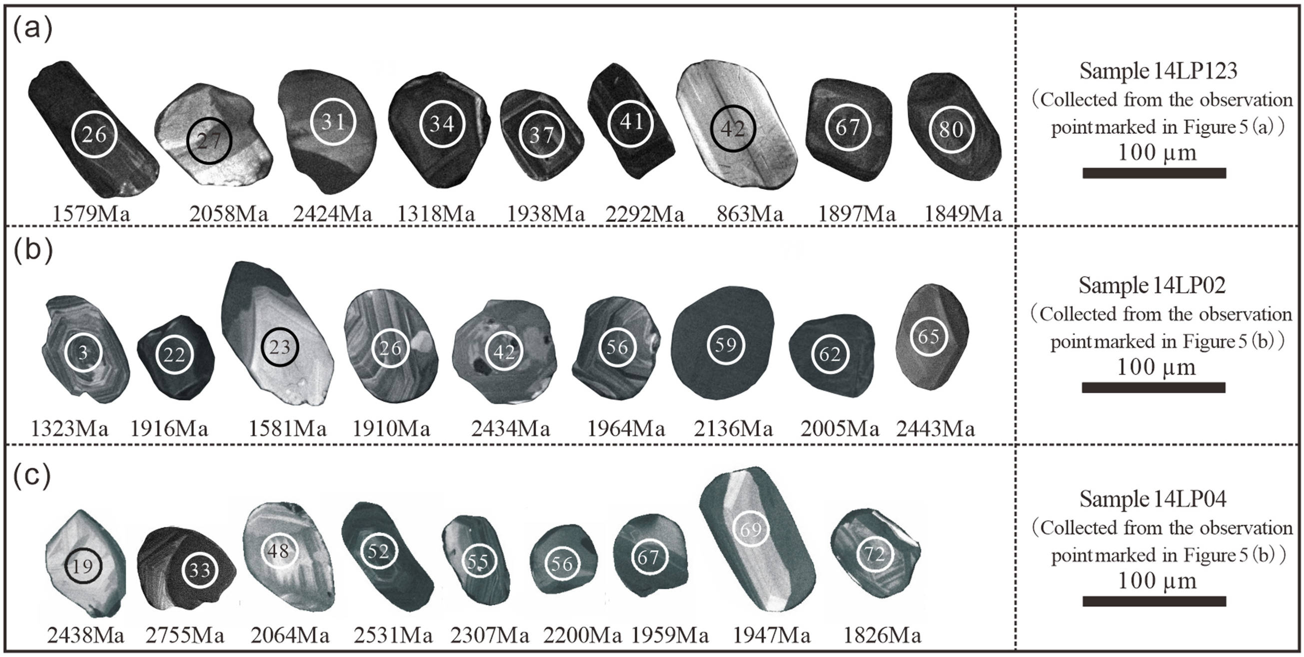

Fig. 7 The cathodoluminescence (CL) image of detrital zircons from the samples 14LP123 **a**, 16LP02 **b**, and 16LP04 **c**. The circle in the figure represents the location of the measuring point, the number in the circle represents the number of the measuring point, and the number around the zircon represents the age value of the corresponding measuring point (Ma)

The period after 753 Ma and before Sinian corresponds to the Neoproterozoic Nanhua System (780–635 Ma) in the 2014 edition of "China Stratigraphic Table", and the Neoproterozoic extension in the 2018 edition of "International Chronological Table" Department (1000–720 Ma). Therefore, based on the U–Pb dating results of detrital zircon in the Changqing low-grade clastic metamorphic rocks, we classify the Changqing low-grade clastic metamorphic rock strata into the Neoproterozoic Nanhua System. Due to the integration and transition of the low-grade clastic metamorphic rock and the Changqing low-grade metamorphic carbonate rock, the entire Changqing low-grade clastic metamorphic rock-carbonate rock can be classified as the Nanhua System. In other words, the low-grade clastic metamorphic rock-carbonate rock of the original Xiong'er Group should be classified as the Nanhua System. The Nanhua System in China is mainly distributed in South China and the Tarim Basin (for example, Yin et al. 2003; Feng et al. 2004; Lu et al. 2008; Gao et al. 2013; Hu et al. 2022; Gou et al. 2022). In North China, only a few Nanhua systems are distributed in eastern Liaoning and eastern Shandong, such as the Qiaotou Formation, the Changlingzi Formation, the Yingchengzi Formation in eastern Liaoning, and Fuzikuang Formation in eastern Shandong, Mashan Formation, etc. (Gao and Chen 2003; Tang et al. 2009). So far there has been no report about the Nanhua system on the southern margin of the NCC. Therefore, the Nanhua strata identified in this article in the southwest of the Ordos Block may be the first Nanhua strata exposed on the southern margin of the NCC.

Magmatism in rift environments and moraine rocks in cold climate environments are commonly developed in the Hanhua System in the Yangtze and Tarim blocks. Magmatism is the structural response to the breakup of the Rodina supercontinent, and moraine rocks are the sedimentary response to the "snowball Earth" (for example, Wang and Li 2003; Wu et al. 2019). In this paper, we proposed the South China system shallow metamorphic clastic rock field determined in the southwest of Ordos block, indicating that although there are relatively few geological records preserved, there are the structural and sedimentary responses in the North China Craton to the breakup process of Rodina supercontinent and the "snowball Earth". Our results provide new clues for this geological process.

5.2 Provenance characteristics of Changqing low-grade clastic metamorphic rocks

Clastic zircons usually preserve the age records of rocks that once existed in the source area. They are one of the main ways to explore the formation and evolution of the NCC (Chen et al. 2008; Li et al. 2009; Hu et al. 2009, 2013; Wan et al. 2010; Diwu et al. 2011, 2012, 2013; Geng et al. 2011; Hu et al. 2012; Wang et al. 2013; Ma et al. 2016). By comparing the age spectrum characteristics

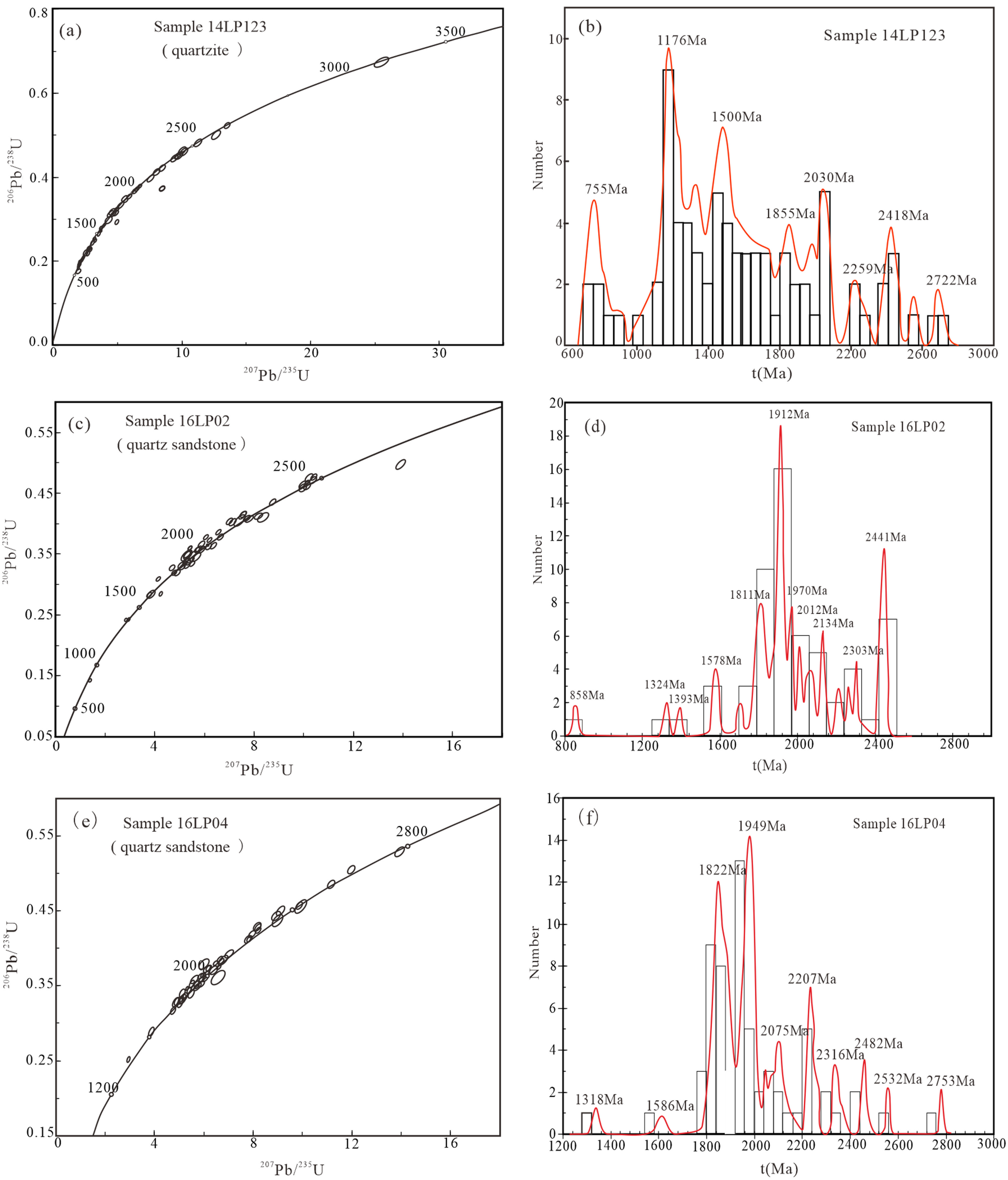

Fig. 8 The Concordia diagrams and histograms of zircon U–Pb dating for samples 14LP123 **a**, **b**, 16LP02 **c**, **d**, and 16LP04 **e**, **f**

of the detrital zircon with the age spectrum of geological events in the surrounding geological block, it is possible to reveal the characteristics of the provenance area.

The detrital zircon U–Pb dating analysis of three samples of low-grade clastic metamorphic rocks was combined and analyzed. The overall analysis reflected nine age peaks: 2755–2722 , ~ 2535, ~ 2438, 2302–2211, ~ 2075, 1952–1823, 1584–1499, 1318–1189, and 856–762, of which 1952–1823, ~ 2438, ~ 2075, and 2302–2211 Ma were several obvious age peaks (Fig. 9). The ages at multiple peak periods reflect that the provenance of this set of low-grade clastic metamorphic rocks is relatively complex.

The peak ages reflected almost all major geological events experienced by the NCC basement since the Neoarchean, including (1) ~ 2.7 Ga large-scale continental crust growth; (2) ~ 2.5 Ga Archaean micro-continental crust splicing welding, continental crust transformation and accretion (Diwu et al. 2011; Zhai and Santosh 2011; Zhai 2011, 2014; Zhang and Sun 2017). A large number of tonalite-trondhjemite-granodiorite rocks and crust-derived granites were formed (Shen et al. 2005; Geng et al. 2010); (3) 2.5–2.3 Ga Ordos Block "tectonic quiet period" (Zhong et al. 2016); (4) 1.95–1.85 Ga Kongzi belt and the central orogenic belt were formed, and the basement of the NCC was cratonized (Zhao 2002, 2009; Zhai and Peng 2007; Zhai 2011; Zhong et al. 2016; Li et al. 2016; Zhang et al. 2018); (5) extension event corresponding to the Xiong'er Group from 1.80 to 1.75 Ga (Zhao 2004) and 1.80–1.78 Ga (Zhai et al. 2014). The age peaks shown in Fig. 9 correspond to the above-mentioned important geological events. However, some age peaks were difficult to correspond to. This indicates that the southwestern part of the Ordos Block was also affected by the tectonic structure of the neighboring areas when the clastic rocks of the Nanhua System of Neoproterozoic were deposited. The obvious influence is consistent with the state at the intersection of multiple tectonic units.

The peak age values of these nine periods had good correspondence with the Precambrian zircon age of the Ordos Block and surrounding West Qinling, Longshan, etc., but mostly similar to the age spectrum of the Changcheng clastic rocks in the basement of the Ordos Block (Fig. 10), it shows that the geological age corresponding to the Changcheng System is the late Paleoproterozoic (1800–1600 Ma), reflecting that the basement evolution of the study area and the Ordos Block has a certain degree of synchronization. Alternatively, the basement rocks of the Ordos Block and the Longshan Group may be the main source area of this set of low-grade clastic metamorphic rocks, and the Qinling group and other groups may have provided some detritus material.

5.2.1 Late Neoarchean age group (2755–2722 Ma and ~ 2535 Ma)

This peak age corresponded well to the zircon ages of the clastic rocks of the Changcheng System of Meso-Proterozoic in the base rocks of the Ordos Block (Fig. 10b), reflecting that such rocks could be an important source area of these low-grade clastic metamorphic rocks.

The age peaks of 2755–2722 Ma were roughly equivalent to the age values of tonalite-trondhjemite-granodiorite rock (TTG) in the Lu mountain, Zhongtiao mountain, and Xiaoqinling areas in the southern NCC (Zhang and Sun 2017). The age peak of ~ 2535 Ma was comparable to the widely developed magmatic metamorphic event of ~ 2.5 Ga in the base of the North China Block (Zhang et al. 2018), which is consistent with the tectonic evolution of the NCC in the Neoarchean. The NCC experienced a large-scale continental crust growth in the middle of the Neoarchean (~ 2.7 Ga). At ~ 2.5 Ga, the Archean microcontinents were spliced and welded, and the continental crust was strongly modified and underwent accretion (Diwu et al. 2011; Zhai and Sanotosh, 2011; Zhai 2011, 2014; Wang and Zhang 2016), forming a large amount of TTG and crust-derived granite (Geng et al. 2010), leading to the first cratonization process of the NCC (Zhai 2008, 2011).

5.2.2 Early Paleoproterozoic age group (~ 2438 Ma, 2302–2211 Ma)

This age group was relatively good with the zircon ages of the clastic rocks of the Changcheng System of Mesoproterozoic (Fig. 10b), Qinling Group-Kuanping Group (Fig. 10c, d), and Longshan Group (Fig. 10e) at the base of the Ordos Block. Indicates that the Ordos Block, the North Qinling, and the Longshan tectonic belt may all be source areas of the low-grade clastic metamorphic rocks. This also means that the North Qinling and Longshan structures may be certain sediment transport channels between the belt and the study area. The strata between 2.47 and 2.35 Ga at the bottom of the Paleoproterozoic NCC were generally missing, reflecting a quiet period in the evolution history of the NCC (Zhong et al. 2016; Yang et al. 2018), and tectonic activities within the NCC may be mainly confined to the edge of the plot. On the northern and eastern margins of the Ordos Block, continental margin arc granites related to the subduction of the Paleoproterozoic (2.2–2.0 Ga) oceanic subduction that was developed (Zhang et al. 2018). The 2.2–1.9 Ga volcanic rocks of the NCC have double peaks. The characteristics of volcanic rocks indicated that the Craton might have experienced strong extensional activities starting from 2.2 Ga (Yang et al. 2018). The Yanliao

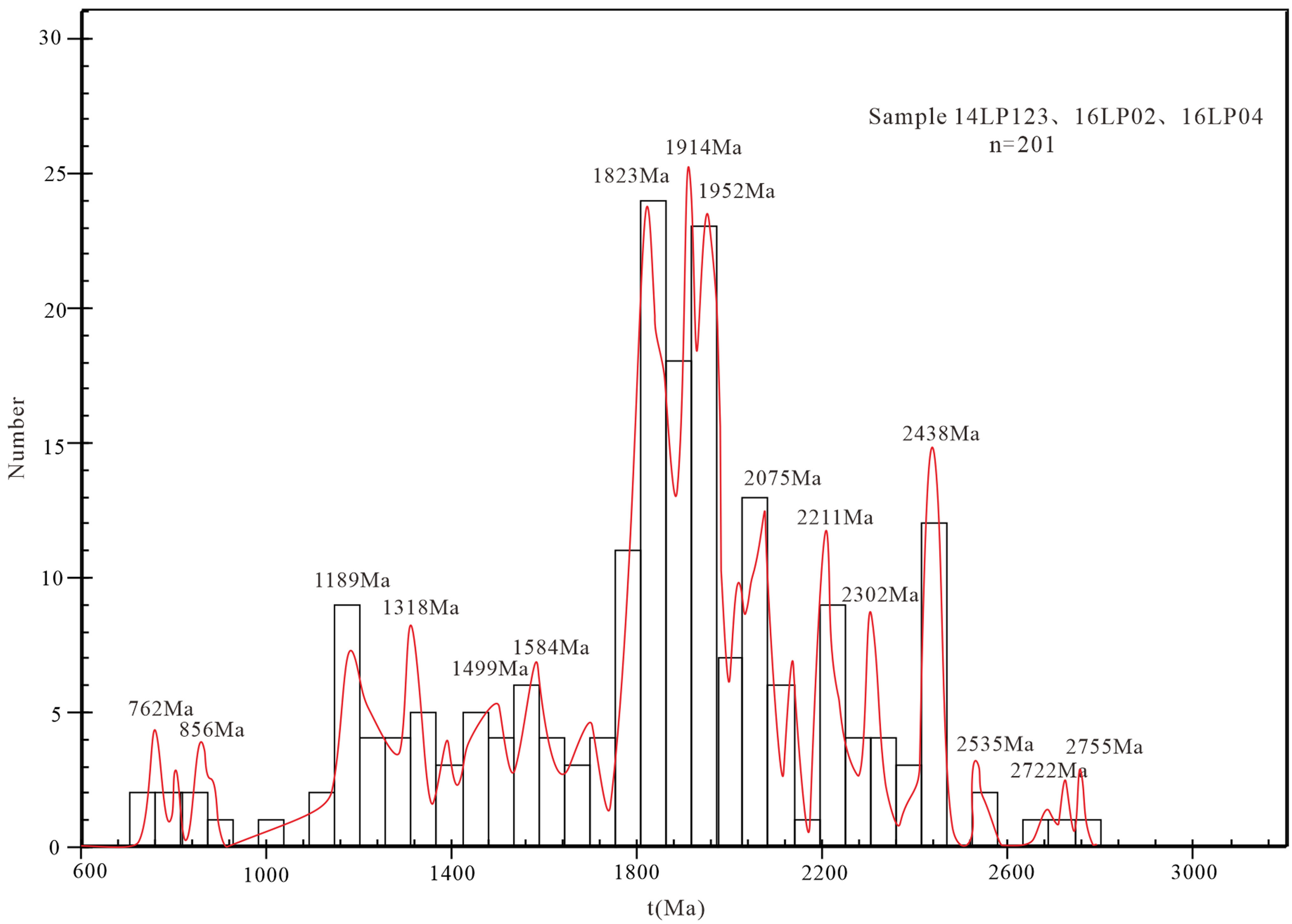

Fig. 9 Histogram of U–Pb dating results of clastic zircons from Changqing low-grade metamorphic clastic rocks

rift trough and Xiong'er rift trough began to develop in the northern and southern margins of the NCC (Zhai et al. 2014).

5.2.3 Paleoproterozoic age group (~ 2075 Ma and 1952–1823 Ma)

This age group was in the zircon ages of the parametamorphic rocks of the Ordos basement and the Changcheng system clastic rocks (Fig. 10a, b), the Qinling, Kuanping (Fig. 10c, d), and the Longshan rock groups (Fig. 10e). All had corresponding reflections, suggesting that they may have a common source area.

During this period, strong tectonic events occurred within the NCC, which resulted in the cratonization of the basement of the NCC. The Yinshan Block and the Ordos Block merged to form the western land block at ~ 1.9 Ga, and the western land block and the eastern land block merged at ~ 1.85 Ga to form the unified basement of the NCC and finally completed the cratonization process of the basement of the NCC (Zhao and Sun 2002; Zhao 2009; Zhai 2011; Li et al. 2016; Zhong et al. 2016; Wang and Zhang 2016; Zhang et al. 2018).

5.2.4 Middle-Neoproterozoic age group (1584–1499 Ma, 1318–1189 Ma, and 856–762 Ma)

The age at this period was quite different from the age spectrum characteristics of the basement metamorphic rocks and Longshan rock group in the Ordos Block shown in Fig. 10, but it was similar to the age spectrum characteristics of the Qinling and the Kuanping rock groups. It reflects that the source rock of the low-grade metamorphic rock may have been the source area of this period similar to the Qinling rock group and the Kuanping rock group, or the Qinling rock group and the Kuanping rock group, directly

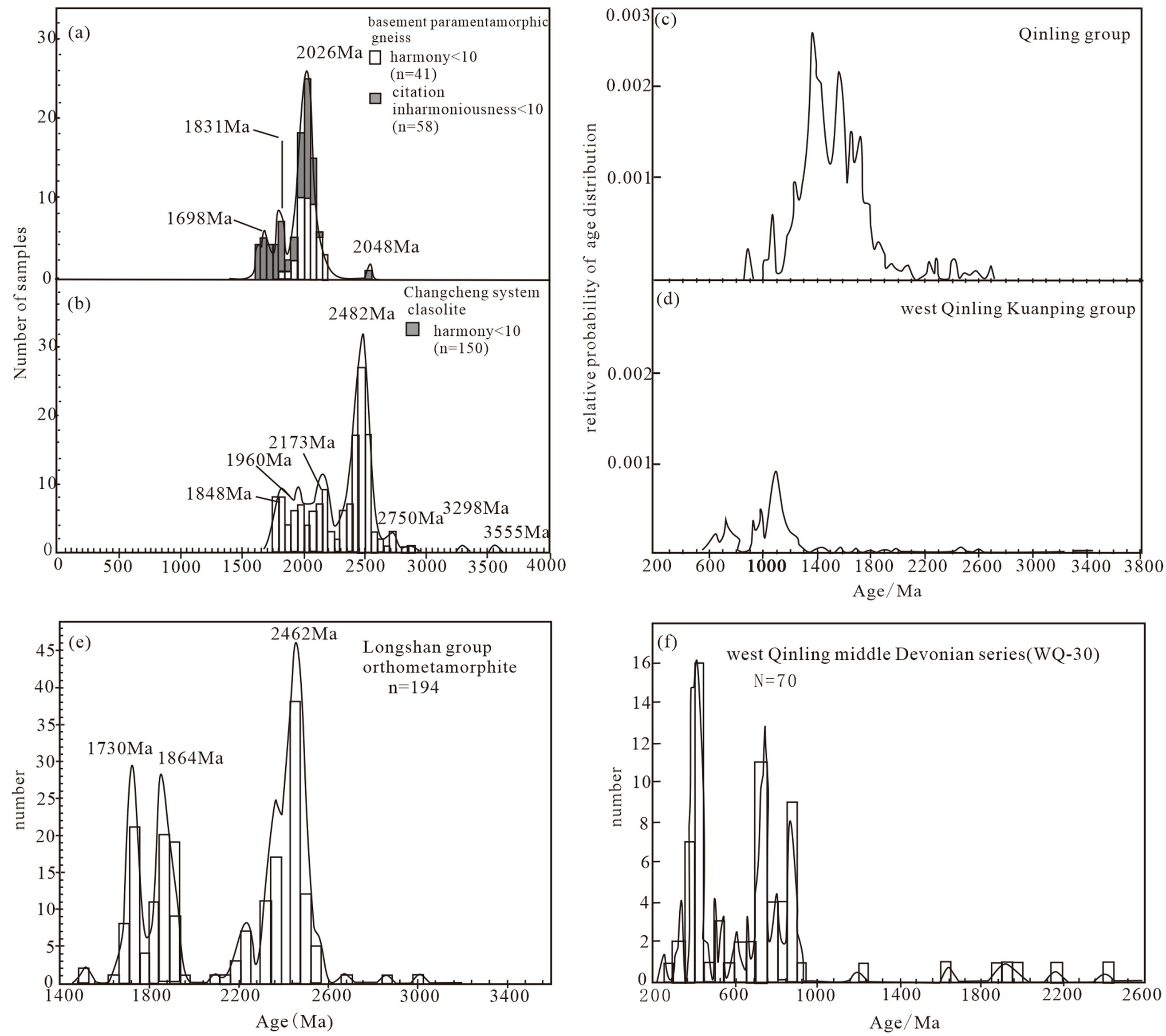

Fig. 10 Zircon age histograms of the tectonic units around the study area. **a**, **b** Zircon age histograms of parametamorphic gneiss and clastic rocks of Great Wall System of Mesoproterozoic in the Ordos basement (according to Zhang et al. 2018); **c**, **d** Zircon U–Pb age histograms of the Qinling rock group in the Qinling orogenic belt and the Kuanping rock group in the West Qinling (according to Gao et al. 2015);**e** Zircon U–Pb age histogram of orthometamorphic rocks in the Longshan Group (according to Xu 2018); **f** U–Pb age histogram of detrital zircons from the Middle Devonian in the West Qinling (according to Chen et al. 2008)

providing the sedimentary source for the study area. The age spectrum of this period was inconsistent with the age spectrum of the Ordos basement rock, implying that the basement of the Ordos Block may no longer have regional provenance characteristics at this time. There were no longer any magmatic events or metamorphic events with regional characteristics. In fact, the NCC including the Ordos Block was basically in a stable state after the late Paleoproterozoic (1.9–1.8 Ga) cratonization (Zhao and Sun 2002; Zhai 2008; Zhao 2009; Li et al. 2016; Wang and Zhang 2016; Zhang et al. 2018). Yanliao rift trough and Xiong'er rift trough of 1700–820 Ma developed only in the north and south margins (Zhai et al. 2014), with the study area located outside the rift trough of the Xiong'er Group in the southern margin and less affected.

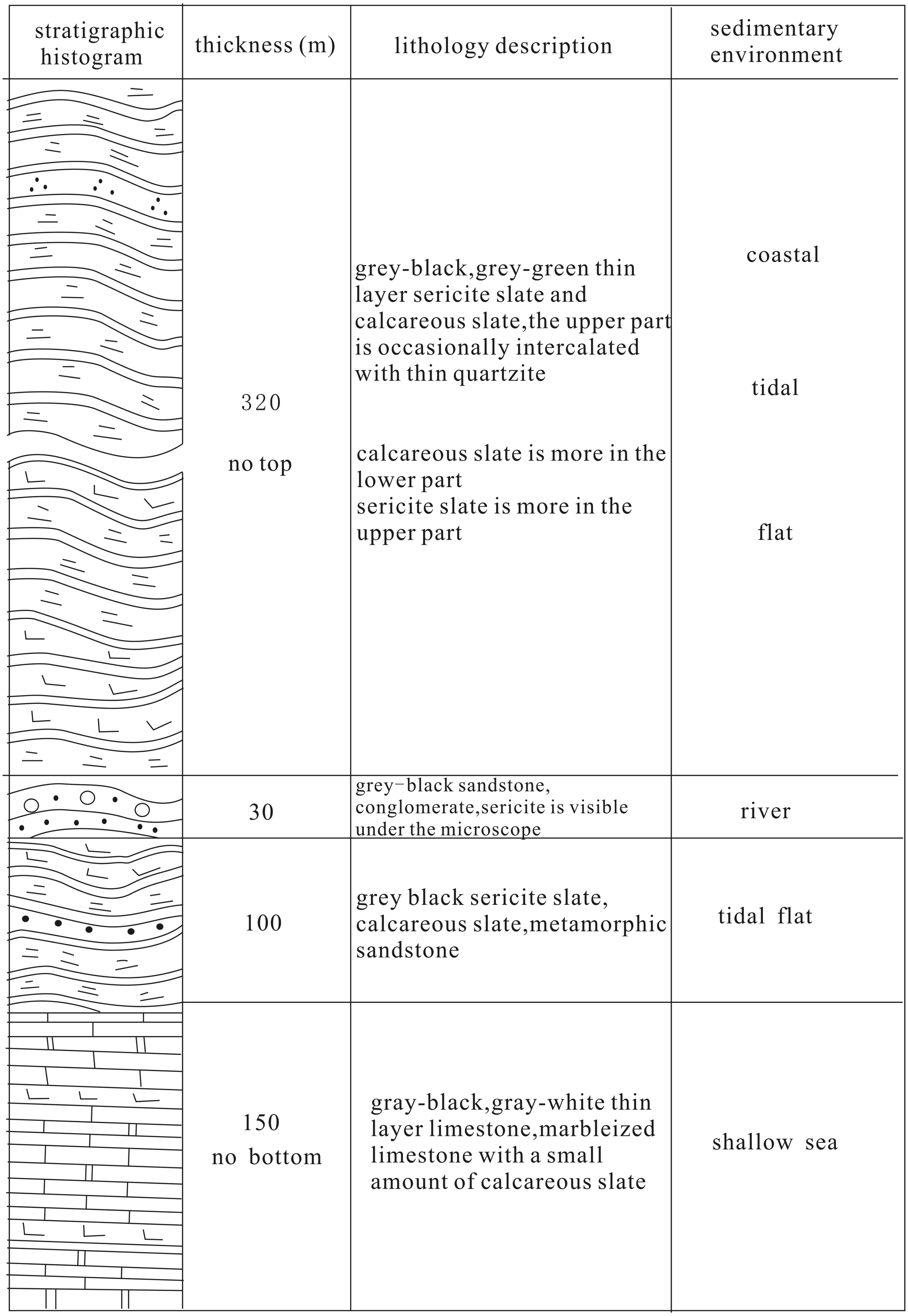

Fig. 11 Stratigraphic histogram of Changqing Nanhua system. The formation thickness in this figure is estimated

5.3 Sedimentary environment characteristics of Changqing low-grade clastic metamorphic rock-carbonate rock

Changqing low-grade clastic metamorphic rock-carbonate rocks were mainly gray-black sericite slate and calcareous slate. A small amount of slate was gray-green, and minor thin gray-black and gray-white layers of gray were exposed in the lower layer of the outcrop and marbled limestone. Gray-black mixed sandstone and complex conglomerate with a thickness of about 30 m were exposed as well. No sedimentary structures such as wave marks and oblique bedding were observed in the rocks. It is speculated that the sedimentary facies markers have been modified during the process of metamorphism. The sedimentary environment of the rocks was inferred based on the original rock, and the overall reaction was a sedimentary sequence from bottom to top and seawater from deep to shallow (Fig. 11). The gray-black and gray-white thin limestone at the bottom should be formed in a Low-grade clastic-sea environment. The original sericite, calcareous slate, and thin sandstone and quartzite strata should be thin mudstone and carbonate evaporite. The sedimentary environment of this kind of rock is inferred to be the coastal tidal flat sedimentary environment. The sedimentary environment of 30 m thick sandstone and conglomerate intercalation was unique. The gravel composition of the conglomerate was complex, with certain rounding and no sorting, showing the characteristics of river sedimentation, and indicating that the sea level in the area had dropped significantly at that time. Consequently, the original coastal tidal flat environment became a river environment. Moraine rocks generally developed in the Nanhua System in southern China. Perhaps the fluvial conglomerates in the Changqing Nanhua System developed at the same time when the Nanhua Moraine rocks in southern China developed (for example, Yin et al. 2003; Feng et al. 2004; Hu et al. 2022; Gou et al. 2022). Large-scale glacial action had led to a drop in sea level, which led to changes in the sedimentary environment of the Changqing Nanhua System. This issue needs to be further studied in the future.

During the Nanhua Period, the plate subduction of the Qinling area mainly occurred in the South Qinling, which had no obvious influence on the study area. From 760 to 680 Ma, the southern Qinling underwent plate subduction in two places at the same time. The Shangdan Ocean Basin slowly subducted southward along the northern part of the Douling Block, and in the southern part of the Xiaomoling Block, an oceanic plate subducted northward along the Fenghuangshan suture zone. These two plate subductions led to the widespread development of volcanic and sedimentary rocks in the Shangwudang Group and Yanlinggou Group (Dong et al. 2016).

The Nanhua deposits in the study area were likely affected by the Neoproterozoic-Early Cambrian rifting in the North Qilian Ocean Basin to the west. During the Neoproterozoic-Early Paleozoic, the North Qilian Ocean, Saishiten-Xitieshan Ocean, and the East Kunlun Ocean began to crack, and the Nanhua-Sinian Baiyangdong Group was deposited on the Central Qilian Block. The Baiyangdong Group is mainly a set of intracontinental rifted basin deposits (Jiang et al. 2014).

Based on the U–Pb dating results of the clastic zircons in the Changqing low-grade clastic metamorphic rocks, this work constrains the deposition time of this set of strata to the Neoproterozoic Nanhua Period. And not far from this set of low-grade clastic metamorphic rocks, the Qingbaikou Guandaokou Group was exposed in the southwest of Fengjiashan Reservoir and on the Miaopoli section of Qishan. The sedimentary environment was different, but it was similar to the sedimentary environment of argillaceous limestone of the Guandaokou Group in the southwest of Fengjiashan Reservoir. From the Guandaokou Group to the Nanhua System in the southwest of Fengjiashan Reservoir, the sedimentary environment had a certain continuity.

The Guandaokou Group in the southwest of Fengjiashan Reservoir was dominated by platform marginal facies argillaceous limestone, while the Guandaokou Group in the Miaopolli section was dominated by platform facies carbonate deposits. Thus, when the Guandaokou Group and this set of Nanhua System clastic metamorphic rock-carbonate rocks were deposited (Qingbaikou to Nanhua), the area was located at the southwestern edge of the Ordos Block. In other words, the southwest boundary of the current Ordos Block was the southwest boundary of the Ordos Block from the Qingbaikou Period to the Nanhua Period.

6 Conclusions

(1) Based on the U–Pb dating results of detrital zircons in the Changqing low-grade clastic metamorphic rocks, this study classified the Changqing low-grade clastic metamorphic rock strata into the Nanhua System.

(2) The basement rocks of the Ordos Block and the Longshan Group may be the main source area of this set of low-grade clastic metamorphic rocks, and the Qinling group and other groups may have provided some detritus material.

(3) The southwestern boundary of the current Ordos Block was the southwest boundary of the Ordos Block from the Qingbaikou Period to the Nanhua Period.

Acknowledgements This research was funded by National Natural Science Foundation of China (Grant No. 42072231). The authors thank You Jia, Xu Huan and Li Yifei for the assistance during fieldwork.

Declarations

Conflict of interest The authors declare that we have no conflict of interest. The authors declare that we have no known competing financial interests or personal relationships that could have appeared to influence the work reported in this paper.

References

Chen GX (2019) Research on the tectonic significance of the Proterozoic geological formations in the southwest of the Ordos Block. Northwest University, Kirkland

Chen YL, Wang Z, Luo ZH, Li DP, Zhao JX (2008) Kangding complex Rb-Sr, Sm-Nd isotope system and its significance. Modern Geol 05:707–714

Chen YL, Li DP, Zhou J, Zhang HF, Liu F, Nie LS, Jiang LT, Liu XM (2008) U–Pb ages of detrital zircons in the West Qinling of China and their tectonic significance. Earth Sci Front 15(04):88–107. https://doi.org/10.3321/j.issn:1005-2321.2008.04.011

Chen GX et al (2019) Geological significance of the former Xiong'er Volcanic Belt on the southwestern margin of the North China Craton. Front Earth Sci 13(1):191–208. https://doi.org/10.1007/s11707-018-0694-z

Diwu CR, Sun Y, Liu L, Zhang CL, Wang HL (2010) Disintegration of the Kuanping group in the North Qinling and Neoproterozoic N-MORB. Acta Petrol Sin 26(07):2025–2038

Diwu CR et al (2011) Crustal growth in the North China Craton at ~2.5Ga: evidence from in situ zircon U–Pb ages, Hf isotopes and whole-rock geochemistry of the Dengfeng complex. Gondwana Res 20(1):149–170

Diwu CR, Sun Y, Liu YJ, Han W, Dai MN, Li YX (2011) The composition of the quartz sandstone source area of the Changlongshan formation in the Liujiang area of Qinhuangdao: evidence from U–Pb-Hf isotope of detrital zircon. J Rock Mineral 30(01):1–12

Diwu CR, Sun Y, Wang Q (2012) Crustal growth and evolution of the North China Craton: enlightenment from the Hf isotopic composition of zircons from modern river detrital. Acta Petrol Sin 28(11):3520–3530. https://doi.org/10.1144/pygs2012-327

Diwu CR, Sun Y, Gao JF, Fan LG (2013) Exploration of the nature of early Precambrian tectonic-thermal events in the North China Craton: U–Pb–Hf–O isotope composition of detrital zircon in the quartzite of the Tietonggou formation. Sci Bull 58(Z2):2946–2957. https://doi.org/10.1360/csb2013-58-28-29-2946

Dong YP, Santosh M (2016) Tectonic architecture and multiple orogeny of the Qinling orogenic belt, Central China. Gondwana Res 29(1):1–40. https://doi.org/10.1016/j.gr.2015.06.009

Feng LJ, Chu XL, Zhang QR, Zhang TG, Li H, Jiang N (2004) New evidence of deposition under cold climate for the Xieshuihe formation of the Nanhua System in northwestern Hunan China. Chin Sci Bull 49(13):1420–1427

Gao ZJ, Chen KQ (2003) Several geological problems of the Nanhua System in Xinjiang and the Nanhua System in China-commemorating the 100th anniversary of the birth of Mr. Wang Yuelun, his teacher. Geol Surv Res 01:8–14

Gao LZ, Guo XP, Ding XZ, Zong WM, Gao ZJ, Zhang CH, Wang ZQ (2013) Nanhuan glaciation event and its stratigraphic correlation in Tarim Plate China. Acta Geosci Sin 34(1):39–57. https://doi.org/10.3975/cagsb.2013.01.05

Gao S, Chen DL, Gong XK, Ren YH, Li HP (2015) Zircon U–Pb dating in clastic rocks and granites of the Kuanping group in Dongcha area, Tianshui and its geological significance. Earth Sci Front 22(04):255–264

Geng YS, Shen QH, Ren LD (2010) Magmatic events and tectonic thermal regime from the end of Late Archean to the beginning of Paleoproterozoic North China Craton. Acta Petrol Sin 26(07):1945–1966

Geng XL, Gao S, Chen C (2011) Crustal growth in the eastern North China Craton and the Sulu orogenic belt: U–Pb dating and Hf isotopic evidence from modern river detrital zircons. Earth Sci 36(03):483–499. https://doi.org/10.3799/dqkx.2011.050

Gou XF, Feng ZH, Li HZ, Huang YG, Wu J, Cui Y, Ma LF, Wang CZ (2022) U–Pb geochronology and Hf isotope characterization of detrital zircons from Nanhua System of northeastern Guangxi and their constraints on the Southwestern suture zone between Yangtze and Cathaysia blocks. South China Arab J Geosci 15:1769. https://doi.org/10.1007/s12517-022-11047-9

Hu GH, Zhao TP, Zhou YY, Yang Y (2012) Sedimentary age and provenance analysis of the Wushan group on the southern margin of the North China Craton: U–Pb age and Hf isotopic evidence of detrital zircons. Geochemistry 41(04):326–342

Hu B, Zhai MG, Guo JH, Peng P, Liu F, Liu S(2009) LA-ICP-MS U-Pb geochronology of detrital zircons from the Huade Group in the northern margin of the North China Craton a and its tectonic significance. Acta Petrologica Sinica,25(1):193–211

Hu B, Zhai MG, Guo JH, Peng P, Liu F, Liu S (2013) LA-ICP-MSU–Pb ages of detrital zircons from the Huade group on the northern margin of the North China Craton and the tectonic significance. Rock J 29(07):2508–2536

Hu B, Zhai MG, Peng P, Liu F, Diwu CR, Wang HZ, Zhang HD (2013) Late Paleoproterozoic-Neoproterozoic geological events of the North China Craton: evidence from LA-ICP-MS U–Pb chronology of Cambrian and Jurassic Detrital Zircons in Xishan Area, Beijing. Rock J 29(07):2508–2536

Hu QF, Qin Y, Feng ZH, Wan L, Xing QL, Wu J, Xue YF (2022) U–Pb age and Hf isotopic characteristics of detrital zircon from the Nanhua System in Longsheng, Northern Guangxi Province, and their geological significance. Geol J 57(3):950–985. https://doi.org/10.1002/gj.4315

Jiang GL, Zhang SM, Liu KF, Zhang KX (2014) Qilian-Qaidam-East Kunlun Neoproterozoic-Mesozoic sedimentary basin evolution. Earth Sci 39(08):1000–1016. https://doi.org/10.3799/dqkx.2014.091

Li HY, Xu Y, Huang XL, He B, Luo ZY, Yan B (2009) Activation of the northern margin of the North China Craton in the Late Paleozoic: U–Pb dating of detrital zircons and Hf isotopes evidence from the upper carboniferous Taiyuan formation in the Ningwu-Jingle Ba sin, Shanxi. Chin Sci Bull 54(05):632–640. https://doi.org/10.1360/csb2009-54-5-632

Li SZ, Zhao GC, Sun M (2016) Research progress on the Early Proterozoic assembly of the North China Craton and the formation of the Columbia supercontinent. Chin Sci Bull 61(09):919–925

Lu SN, Li HK, Zhang CL, Niu GH (2008) Geological and geochronological evidence for the Precambrian evolution of the Tarim Craton and surrounding continental fragments. Precambrian Res 160:94–107. https://doi.org/10.1016/j.precamres.2007.04.025

Ma MZ, Zhang YX, Jie HQ, Wan YS (2016) U–Pb dating and Hf isotope analysis of detrital zircons from the bottom of the Baiyun Obo group and the Sailin Hudong group on the northern margin of the North China Craton and their geological significance. Acta Petrol Sin 30(10):2973–2988

Pulido N, Kubo T (2016) Source characteristics and strong ground motion during the 2001 El Salvador earthquake. In: Proceedings of the earthquake engineering research conference, vol 26. Japan Society of Civil Engineers, Tokyo, p 533–536

Shen QH, Geng YS, Song B, Wan YS (2005) New information on the surface and deep Archean basement of the North China and Yangtze blocks and the Qinling-Dabie orogenic belt. Acta Geol 05:616–627

Tang F, Yin CY, Gao LZ, Liu PJ, Wang ZQ, Chen SM (2009) Neoproterozoic macrofossil biostratigraphic sequence in the eastern North China Craton. Geol Rev 55(03):305–317. https://doi.org/10.3321/j.issn:0371-5736.2009.03.001

Wan YS, Miao PS, Liu DY, Yang CH, Wang W, Wang HC, Wang ZJ, Dong CY, Du LL, Zhou HY (2010) The formation age and material source of the Gaofan, Hutuo and Dongjiao groups of the North China Craton: SHRIMP U–Pb isotopic chronology constraints of detrital zircon. Sci Bull 55(07):572–582. https://doi.org/10.1360/csb2010-55-7-572

Wang J, Li ZX (2003) History of Neoproterozoic rift basins in South China: Implications for Rodinia break-up. Precambr Res 122(1–4):141–158

Wang JL, Zhang HF (2016) Three-phase tectonic-magmatic events recorded by ancient granulites in the North China Craton. Acta Petrol Sin 32(03):682–696

Wang M, Luo JL, Li M, Bai XJ, Cheng C, Yan LW (2013) Analysis of the source area of sandstone-type uranium deposits in Dongsheng area of Ordos Basin and their tectonic background: evidence from U–Pb age and Hf isotopes of detrital zircons. Acta Petrol Sin 29(08):2746–2758

Wu L, Guan SW, Ren R, Zhang CY, Feng XQ (2019) Neoproterozoic glaciations and rift evolution in the Northwest Tarim Craton, China: new constraints from geochronological, geochemical, and geophysical data. Int Geol Rev. https://doi.org/10.1080/00206814.2019.1700399

Xu KX (2018) Precambrian chronology and geochemistry of the Qin-Qi junction: evidence from the Longshan group. Northwest University, Kirkland

Yang CH, Du LL, Song HX, Ren LD, Miao PS, Lu ZL (2018) Paleoproterozoic stratigraphic division and comparison of the North China Craton. Acta Petrol Sin 34(04):1019–1057

Yin CY, Liu DY, Gao LZ, Wang ZQ, Xing YS, Jian P, Shi YR (2003) Lower boundary age of the Nanhua System and the Gucheng glacial stage: evidence from SHRIMP II dating. Chin Sci Bull 48(16):1657–1662. https://doi.org/10.1360/03wd0112

You J (2016) Chronology, geochemistry and tectonic significance of the Xiong'er group in the Southwestern margin of the Ordos Basin. Northwest University, Kirkland

Zhai MG (2008) Lithospheric mantle and lower crust before Mesozoic destruction of the North China Craton. Acta Petrol Sin 24(10):2185–2204

Zhai MG (2011) Cratonization and the formation of the North China Block. Sci China Earth Sci 41(08):1037–1046. https://doi.org/10.1360/zd-2011-41-8-1037

Zhai MG (2014) Multi-stage crustal growth and cratonization of the North China Craton. Geosci Front 5(04):457–469

Zhai MG, Peng P (2007) Paleoproterozoic tectonic events of the North China Craton. Acta Petrol Sin 11:2665–2682

Zhai MG, Santosh M (2011) The Early Precambrian odyssey of the North China Craton: a synoptic overview. Gondwana Res 20(1):6–25

Zhai MG, Hu B, Peng P, Zhao TP (2014) Magmatism and multi-stage rift events in the Mid-Neoproterozoic North China. Front Earth Sci 21(01):100–119

Zhang RY, Sun Y (2017) Formation and evolution of the Early Precambrian basement in the Southern part of the North China Craton. Acta Petrol Sin 33(10):3027–3030

Zhang CL, Gou LL, Diwu CR, Liu XY, Zhao J, Hu YH (2018) Early Precambrian geological events, properties and their geological significance in the western basement of the North China Craton. Acta Petrol Sin 34(04):981–998

Zhao GC (2009) The metamorphism evolution of the main tectonic units of the basement of the North China Craton and discussion of some issues. Acta Petrol Sin 25(08):1772–1792

Zhao GC, Sun M, Wilde SA (2002) Characteristics of basement tectonic units of the North China Craton and Early Proterozoic assembly. Sci China 32(07):538–549. https://doi.org/10.3321/j.issn:1006-9267.2002.07.002

Zhao TP, Zhai MG, Xia B, Li HM, Zhang YX, Wan YS (2004) Zircon SHRIMP chronology of Xiong'er group volcanic rocks: constraints on the initial time of North China Craton caprock development. Sci Bull 22:2342–2349. https://doi.org/10.1360/csb2004-49-22-2342

Zhong Y, Chen YL, Zhai MG, Ma XD (2016) Stratigraphic correlation, lithofacies and paleogeographic features and geological significance of the Palaeoproterozoic Kongzi series in the western North China Craton. Acta Petrol Sin 32(03):713–726